Master Thesis in Geographical Information Science nr 209

Flood impacts on road accessibility and buildings in Gothenburg during a 100-year rainfall event

Sebastian Daland

2026
Department of
Physical Geography and Ecosystem Science
Centre for Geographical Information Systems
Lund University
Sölvegatan 12
S-223 62 Lund
Sweden

Sebastian Daland (2026). Flood impacts on road accessibility and buildings in Gothenburg during a 100-year rainfall event.

Master degree thesis, 30 credits in Master in Geographical Information Science

Department of Physical Geography and Ecosystem Science, Lund University

Flood impacts on road accessibility and buildings in Gothenburg during a 100-year rainfall event

---

Sebastian Daland

Master thesis, 30 credits, in Geographical Information Sciences Lund University

Supervisor:

Helena Elvén Eriksson

Department of Physical Geography and Ecosystem Science
Lund University

Vidar Glette

Ramboll Urban Planning West
Gothenburg

Acknowledgements

I would like to thank Ramboll in Gothenburg for having me during this project and especially Vidar Glette for being my supervisor, contributing with knowledge and ideas to the project. I would also like to thank my supervisor at Lund University, Helena Elvén Eriksson, for her feedback and for helping me with the structure of the report.

This master's thesis marks the end of my studies, and I am grateful that I chose to study Geographic Information Science as it has further developed my interest in GIS and opened doors to new career opportunities.

Sebastian Daland

Abstract

Urban areas are increasingly exposed to extreme precipitation events, which can disrupt critical infrastructure and damage the built environment. While flood impacts are often assessed separately for buildings or road networks, this study analyses both flood-induced road inaccessibility and building flood risk in Gothenburg using a climate-adjusted 100-year rainfall at both the city scale and the local scale. A network-based service area approach was used to identify inaccessible areas, while building flood risk was assessed using a risk classification matrix based on two factors: exposure ratio and maximum flood depth. The results show that road inaccessibility is most severe in peripheral areas with low network redundancy where limited alternative routes can lead to extensive accessibility loss, whereas the highest building flood risk is concentrated in low-lying and industrial areas. Local-scale case studies revealed how localized flooding disrupts road networks at vulnerable road segments and generates uneven building-level risk that is not visible at the city scale. By integrating road inaccessibility with building flood risk into a combined risk classification, the study identifies areas where flooding is likely to generate the greatest societal consequences, highlighting vulnerabilities that would not be visible from either component alone. Together, these findings demonstrate the importance of multi-scale and integrated flood risk assessments for informing urban resilience planning and guiding climate-adaptive strategies.

Keywords: GIS, urban flooding, road inaccessibility, building flood risk, 100-year rainfall

Table of Contents

List of Figures

List of Tables

1 Introduction

1.1 Background

Extreme weather events, including extreme precipitation, have increased in both frequency and intensity since the 1950s over most land areas, with anthropogenic climate change being identified as the main driver (IPCC, 2023). This trend is expected to continue with additional global warming, as a warmer atmosphere can hold more moisture, leading to more extreme precipitation (Seneviratne et al., 2021). For Europe, the frequency of extreme precipitation events is projected to nearly double for each 1°C of global warming (Myhre et al., 2019). Northern Europe has been identified as a region where these changes will be especially noticeable (Seneviratne et al., 2021), making cities in this region increasingly vulnerable to pluvial flooding.

In Sweden, annual precipitation has increased from approximately 600 mm in 1930 to nearly 700 mm today (Schimanke, 2022) and is projected to continue increasing throughout the century (Sjökvist et al., 2025). Although no clear long-term trends have been identified in the magnitude and frequency of cloudbursts – defined by the Swedish Meteorological and Hydrological Institute (SMHI) as rainfall exceeding 50 mm within one hour or 1 mm per minute – observations indicate a slight increase in annual maximum precipitation since 1881 and an increased frequency of prolonged two-day rainfall events since 1961 (Olsson et al., 2017). Climate projections further suggest that cloudburst intensity will increase over the century, with increases of approximately 10% during 2011–2040 and up to 20% and 40% toward the end of the century under low-emission (RCP4.5) and high-emission (RCP8.5) scenarios, respectively (Sjökvist et al., 2025).

Most low-pressure systems affecting Sweden move in from the west or southwest, resulting in the highest precipitation levels occurring in these regions (SMHI, n.d.-a). Västra Götaland County has been identified as the most affected region by summer cloudbursts between 2009 and 2018 in terms of both the number of events and total estimated impact (Nyberg et al., 2019). This aligns with the findings from Sjökvist et al. (2025) which show that the Swedish west coast experienced the highest number of days with extreme precipitation – defined as more than 20 mm of precipitation within 24 hours – during 1971–2000, averaging six to eight days per year. Climate projections indicate that this region may experience the largest future increases, with the number of days with extreme precipitation potentially doubling toward the end of the century under RCP8.5 (Sjökvist et al., 2025).

Gothenburg, located in Västra Götaland County, lies in one of Sweden's most precipitation-intensive regions and is projected to face some of the largest future increases (Sjökvist et al., 2025). As Sweden's second-largest city, its dense population and critical infrastructure increase its vulnerability to flood-related impacts, which is further exacerbated by its coastal location and proximity to the Göta Älv river. The city has experienced several extreme rainfall events with significant societal consequences. In August 1997, an extreme precipitation event resulted in 113 mm of rainfall within 24 hours, causing widespread road flooding, traffic disruptions, and stranded vehicles (Göteborgs Stad, n.d.-a). Similar events elsewhere in Scandinavia further illustrate the potential consequences of urban flooding. For example, the 2011 cloudburst in Copenhagen, where rainfall intensities exceeded 3 mm per minute for more than 10 minutes and most of the 135 mm of precipitation fell within just two hours (DMI, 2011), causing extensive infrastructure damage and economic losses estimated at 9.4 billion SEK (MSB, 2016). This event corresponded to a 100-year rainfall, defined as a rainfall event with a 1% annual probability of occurrence, which is a common benchmark in flood risk assessments.

Urban areas, including Gothenburg, are particularly vulnerable to pluvial flooding due to the high proportion of impermeable surfaces, which increases surface runoff during intense rainfall. When the capacity of drainage systems is exceeded, excess water accumulates on the surface, affecting both the built environment and societal functioning. Flooded buildings may experience structural damage, moisture-related degradation, and reduced usability, while flooded roads can become impassable, disrupting traffic and emergency services. Research has shown that even relatively shallow inundation depths can result in significant impacts on infrastructure (Huizinga et al., 2017). For buildings, depth-damage curves often start to increase at very small inundation depths, with damage continuing to rise until an upper threshold is reached (Huizinga et al., 2017). For roads, inundation depths of approximately 30 cm have been identified as a critical threshold for safe driving, beyond which vehicle stability, steering, and braking are significantly compromised for most passenger cars (Pregnolato et al., 2017).

In response to increasing flood risk, Sweden has developed a comprehensive flood risk management framework, guided by national and European policy frameworks. The EU Flood Directive (2007/60/EC) requires member states to work towards reducing the adverse consequences of flooding for human health, the environment, cultural heritage, and economic activity (MSB, 2020). In Sweden, the directive is implemented through the Regulation on Flood Risk (Förordningen om översvämningsrisker, SFS 2009:956), which assigns the Swedish Civil

Defence and Resilience Agency (MCF) responsibility for coordinating national flood risk assessments and management planning. County administrative boards are responsible for developing and implementing regional flood risk management plans in accordance with MSBFS 2013:1. To support municipalities, MSB (2017) provide guidelines for cloudburst mapping and flood risk assessments, recommending the use of geographic information systems (GIS) and hydrodynamic modelling to evaluate flood extent, impacts, and mitigation measures.

GIS has become a central tool in flood risk assessments due to its ability to integrate spatial data, model complex relationships, and visualize patterns across multiple scales. Previous studies have applied GIS to assess flood impacts on various urban components, including road networks and buildings. Regarding roads, Papilloud et al. (2020) used GIS to assess flood exposure of road infrastructure by aggregating exposure into grid cells, highlighting spatial patterns of vulnerability at the national scale, while Lin et al. (2024) combined GIS with traffic and topological data to assess segment-level disruptions and congestion in urban areas. Regarding buildings, Paulik et al. (2023) modelled national residential building exposure to flooding using GIS to estimate the quantity and replacement value of homes, whereas Taramelli et al. (2022) focused on individual building losses by integrating hazard and vulnerability data. Together, these studies demonstrate the ability of GIS to support flood risk assessments across multiple urban components and spatial scales.

While previous GIS-based flood studies have typically analysed either building exposure or road network disruptions, few have combined these components to identify areas where multiple impacts coincide. Detailed analyses of flood-induced road inaccessibility within flood affected areas also remain relatively scarce. This study addresses these gaps by integrating network analysis of road inaccessibility with building flood risk analysis for Gothenburg at both the city scale and the local scale. In doing so, the study contributes to improved understanding of urban flood impacts and supports ongoing efforts in flood risk management and climate adaptive urban planning under increasing extreme precipitation.

1.2 Aim & research questions

The aim of this study is to assess flood-induced road inaccessibility and building flood risk in Gothenburg during a 100-year rainfall event at both the city scale and the local scale, in order to evaluate their spatial distribution, combined risk, and detailed patterns within high-risk areas.

The study is guided by the following research questions:

- Which areas in Gothenburg experience the largest flood-induced road inaccessibility at the city scale during a 100-year rainfall event?
- Which areas in Gothenburg experience the highest building flood risk at the city scale during a 100-year rainfall event?
- Which areas in Gothenburg face the greatest combined risk of road inaccessibility and building flood risk at the city scale during a 100-year rainfall event?
- Which spatial patterns characterize road inaccessibility and building flood risk within high-risk areas at the local scale?

2 Study Area

Gothenburg (57°42'N, 11°58'E) is located on the Swedish west coast and is the second largest city in Sweden with 608 993 inhabitants (SCB, 2025). It is one of the fastest-growing cities in the country and the population is projected to increase by 104 700 inhabitants by 2050 (Göteborgs Stad, n.d.-b). The city is concentrated in the central part of the municipality where built-up areas and infrastructure are most dense, gradually decreasing toward the outskirts. The study area covers the mainland of Gothenburg, excluding the surrounding islands (Figure 1).

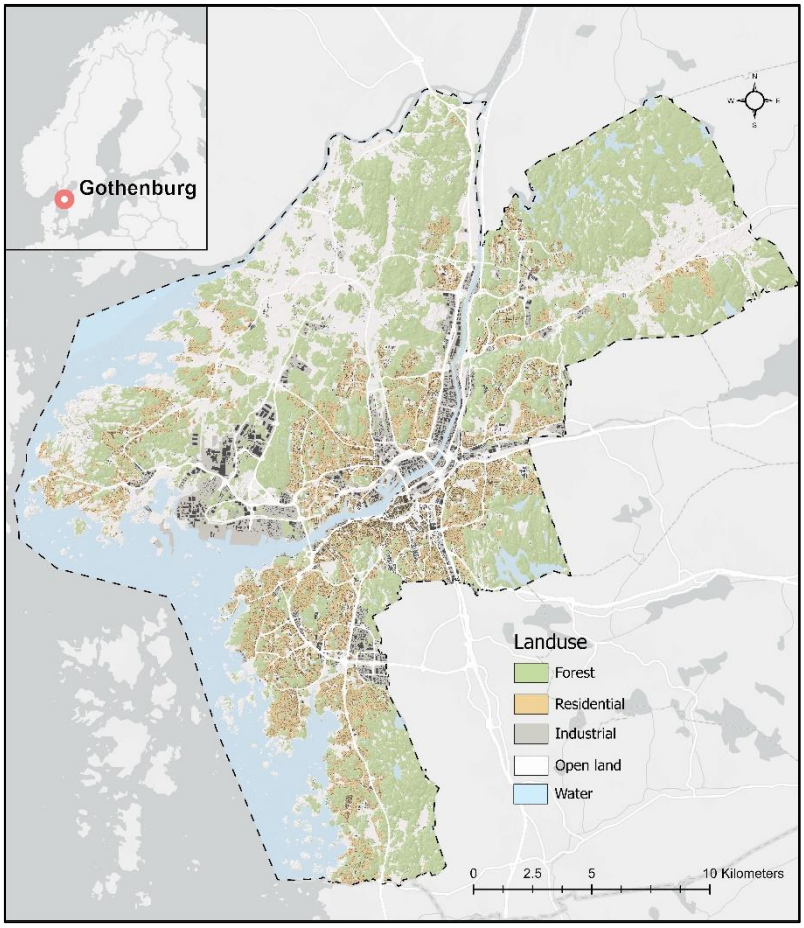

Figure 1. Overview map of Gothenburg's mainland.
Basemap: ESRI Light Gray Canvas.

Gothenburg has a temperate oceanic climate characterized by cool summers and relatively mild winters for its latitude, classified within the *Cfb* category in the Köppen Geiger climate classification (Beck et al., 2023). Average monthly temperatures range from 0.7°C in February to 18.2°C in July, with an annual mean temperature of 8.9°C (SMHI, n.d.-b). The city receives an average annual precipitation of 917 mm, with August and October being the wettest months, each averaging around 90 mm of precipitation. The most extreme rainfall events typically occur in July and August (Göteborgs Stad, n.d.-a).

3 Material & methods

This section provides an overview of the data used in this study, followed by a more detailed description of the 100-year flood data, the road preprocessing, and the GIS analyses, including a network analysis, a building risk analysis, and a combined risk evaluation.

3.1 Data

The data used in this study are summarized in Table 1 and referenced in SWEREF99 TM (EPSG:3006). The 100-year flood raster is described in more detail below as it is derived from a hydrodynamic model and represents the primary dataset, providing simulated flood conditions for the analyses.

Table 1. Overview of data used in this study.

Data	Source	Format	Description
100-year flooding	Göteborg Kretslopp och Vatten (2021a)	Raster (4 x 4 m)	Simulated flooding during a 100-year rainfall event.
Buildings	Lantmäteriet (2024)	Vector polygons	Building footprints with building type classification.
Roads	Trafikverket (2025)	Vector lines	Road network with traffic related attributes.
Bridges and tunnels	Trafikverket (2022)	Vector lines	Overpasses, underpasses, and tunnels on road sections.
Watercourses	Lantmäteriet (2024)	Vector lines	Watercourses narrower than 6 meters.

3.1.1 100-year flood raster

The 100-year flood raster represents the simulated flood situation during an event with a 1% annual probability of occurring given the historical record of rainfall, following the methodology from the Swedish Civil Defence and Resilience Agency (MSB, 2017). This event serves as a modelling scenario to assess potential flood impacts.

The flood raster used in this study is produced by Gothenburg Recycling and Water (Göteborg Kretslopp och Vatten 2021b) and is based on fully coupled 1D-2D hydrodynamic simulations (MIKE) to simulate how extreme precipitation interacts with urban surfaces, sewer networks,

and rivers. It integrates elevation, land use, soil types, rainfall and sewer systems to calculate runoff, infiltration, surface flow, sewer flow, and river flow within a single integrated system. Among the input parameters, elevation is particularly influential in determining local water accumulation and flow paths, while land use and soil types decide how rainfall is divided between infiltration and surface runoff. Rainfall intensity drives the magnitude of flooding, and sewer networks determine how efficiently excess water is transported away. Based on a climate-adjusted 100-year rainfall event where a climate factor of 1.2 (representing 20% increase) is applied to account for projected future increases in rainfall intensity and focusing on the most intense 30-minute peak within a 6-hour period, the hydrodynamic simulations produce water depths, flow paths, and flood duration. Only the simulated water depth is used in this study, as it is the primary indicator of flood severity in relation to road passability and potential building damage.

The flood raster is based on hydrodynamic simulations representing the flooding situation at the time of the height scanning and the land-use mapping conducted in 2017. Areas with significant changes after this might therefore show misleading results and should be interpreted with caution. The elevation data is derived from lidar scanning, providing high-resolution terrain information for accurate surface flow. The resulting raster has a 4 x 4 m spatial resolution, which was chosen to maintain reasonable computation times while still capturing urban structures in sufficient detail. Further information about the hydrodynamic modelling framework can be found in the model documentation (Göteborg Kretslopp och Vatten, 2021a).

At the municipal level, the flood raster serves as the official flood map for Gothenburg and forms the basis for planning and risk assessments. The hydrodynamic modelling approach itself is not evaluated within the scope of this thesis. While different approaches to flood modelling exist, the focus here is on analysing the impacts derived from the raster dataset rather than evaluating modelling techniques.

3.2 GIS methodology

All analyses are based on the 100-year flood raster with a 4 x 4 m resolution and are conducted at two spatial scales. The *city scale* represents a generalized approach in which roads and buildings are aggregated to capture overall spatial patterns across Gothenburg, whereas the *local scale* represents individual roads and buildings to examine fine-scale spatial dynamics within selected areas. This distinction acknowledges well-established scale effects

in spatial analysis, whereby aggregation can influence the resulting spatial patterns and their interpretation (Openshaw, 1984).

3.2.1 Network-based service area analysis of road inaccessibility

A service area analysis is a type of network analysis that identifies all network segments reachable from a given location within a specified impedance, where impedance represents the cost of travel, such as distance or time (Esri, n.d.-a). This type of analysis is commonly applied to assess accessibility and disruptions in transportation systems during extreme events, such as flooding, as it explicitly represents network connectivity and illustrates how flooded road segments interrupt that connectivity (Alabbad et al., 2024; Yin et al., 2020). In this study, the impedance cutoff was set sufficiently high to ensure that the entire road network would be reachable from the defined starting points.

All flooded areas included in this analysis have a water depth of at least 30 cm, extend over a minimum of 10 m of continuous road, and cover at least 500 m^2. The 30 cm depth threshold was selected based on previous research identifying this as a critical threshold for safe driving (Pregnolato et al., 2017). The minimum length and area thresholds were applied to exclude spatially limited flooding that is unlikely to represent meaningful barriers to road accessibility.

Network preprocessing

To conduct the service area analysis, a network was first created with the following restrictions:

- Flooded road segments prohibited
- Bridges and tunnels always traversable
- Elevation-aware end-point connectivity to prevent false intersections
- Forbidden direction applied on major roads; both directions allowed on minor roads

Directional restrictions were applied only to major roads (classes 0–3 in the functional road classification of the Swedish Transport Administration), assuming that these roads are unlikely to be used against the designated traffic direction even during disruptive flood conditions. Minor roads (classes 4–9 in the same classification) were treated as bidirectional to reflect the greater flexibility typically possible within local street networks under such conditions.

To ensure that the network accounted for all flooding barriers prior to the service area analyses, a pre-processed “hard-cut” network was created. Instead of using dynamic barriers in the Network Analyst extension, where the service area analyses are conducted, flooded road segments were removed directly from the network using an erase operation between the road dataset and the flood polygons. Dynamic barriers are temporary restrictions that can be applied

during an analysis without permanently modifying the network, but the hard-cut approach was chosen because several criteria – such as the minimum flooded road length and the traversability of bridges and tunnels – could not be consistently implemented using dynamic barriers.

Additional preprocessing steps were required for elevated and underground structures. For bridges, short segments combined with the flood resolution of 4 x 4 m made false flooding likely. A 20-meter buffer was therefore applied before and after bridges to reduce this effect. Smaller bridges not included in the bridge dataset were identified by intersecting flooded road segments with watercourses, assuming that any road crossing a watercourse corresponds to a bridge structure. For tunnels, flood polygons intersecting tunnel entrances were removed entirely, as tunnel openings typically include engineered drainage systems to manage local flooding. Each tunnel was manually validated to ensure that only the relevant flood polygons were removed.

City-scale accessibility analysis

The city-scale analysis was conducted using a single, centrally located starting point for the service area analysis, which was manually verified to ensure that it was not situated within a flooded area. This verification was necessary to ensure that the starting point was located on a connected and traversable part of the network, allowing the service area analysis to represent the full extent of reachable roads. In this analysis, all flooded streets had been removed entirely from the network during the preprocessing, effectively acting as barriers, so that the resulting service area reflects the portions of the network that remain accessible despite the flooding. Inaccessible roads were subsequently identified by removing the service area from the road network, leaving only those segments that could not be reached from the central starting point. This procedure enables the identification of areas that are completely disconnected from the network due to flooding (Figure 2).

To reduce edge effects in the analysis, a 2000-meter buffer was applied to the road network beyond the municipal boundary to avoid underestimating accessibility near the study area edges. The buffer distance was selected to ensure that major roads crossing the boundary remained connected within the network.

Figure 2. Illustration of the service area analysis used to determine accessible and inaccessible roads.

Following the service area analysis, the identified inaccessible roads were further filtered to focus on meaningful disruptions. Continuous segments of inaccessible roads exceeding 200 meters in length and containing at least 5 nearby buildings of relevant types (residential, commercial, industrial, or public) within 50 meters were classified as inaccessible areas. These thresholds ensure that inaccessible areas represent continuous road networks with sufficient surrounding building exposure. The 200-meter length criterion excludes small isolated segments, while the requirement of at least 5 nearby buildings emphasizes areas likely to affect residents, workplaces, or essential services.

Centroids were generated for all inaccessible areas for visualization purposes. Each centroid was symbolized using graduated symbols based on a combined risk score. Road length and building count were normalized to a 0–100 scale using min-max normalization and combined using weights that emphasize human exposure (0.6 x buildings, 0.4 x roads), reflecting the assumption that areas with more buildings are likely to affect more people than road disruptions alone. Logarithmic scaling (log10(RiskScore + 1)) was applied to reduce the influence of extreme values and improve visual differentiation.

Local-scale accessibility analysis

The local-scale analysis applied an iterative approach to progressively map road accessibility beyond individual flood barriers, enabling accessibility patterns to be captured at a finer scale. The two areas with the largest and most critical inaccessibility identified in the city-scale analysis were selected as case studies, and the approach was applied independently within each area. To implement the approach, flooded road segments were first identified by intersecting flood polygons with the road network and grouping continuous flooded segments into barriers. These barriers were then integrated into an updated road network prepared for the service area analyses.

Initial starting points were manually established immediately beyond the first flood barrier responsible for the identified inaccessibility, ensuring that each iteration began just beyond previously accessible parts of the network. In each iteration, a service area was generated from the current set of starting points to identify accessible areas and detect the next flood barriers. Remaining accessible roads within the network were identified by removing both current barriers and previously mapped service areas. New starting points were then established immediately beyond the identified barriers to initiate the next iteration. This process continued until all reachable parts of the study area had been traversed (Figure 3).

The four recurring steps can be summarized as follows:

1. Generate service area
2. Identify next flood barriers
3. Extract remaining accessible roads
4. Establish new starting points

Figure 3. Illustration of the iterative service area approach for mapping road accessibility beyond flood barriers.

3.2.2 Building flood risk analysis

Risk classification

To assess building-level flood impacts, a building flood risk analysis was conducted. The risk analysis classifies buildings into four classes, where Risk-1 represents the lowest and Risk-4 the highest risk of flood-related impacts. Two factors were evaluated to assign buildings to the appropriate risk class: (1) the proportion of each building's footprint (%) that becomes flooded and (2) the maximum flood depth along the building footprint. These two factors were selected to capture both the spatial extent and intensity of the flooding affecting each building.

In order to obtain values, points were distributed around each building footprint at 1-meter intervals, and flood-depth values were extracted at each point in order to calculate both the flooded proportion of the footprint and the maximum flood depth. The points were buffered 4 meters outward from the buildings to reduce edge uncertainties caused by the 4 x 4 m 100-year flood raster and thus obtain more accurate estimates of flood exposure. An illustration of the building flood risk methodology is shown in Figure 4.

The classification matrix (Table 2) specifies how the calculated maximum flood depth and building exposure ratio are combined to assign each building to a flood risk class. Flood depth is classified using a minimum threshold of 10 cm, commonly applied in building-level flood risk analyses, with depth intervals aligned with those used in other 100-year rainfall analyses in Swedish cities (DHI, 2014; Structor, 2017; WSP, 2023). Building exposure is classified using exposure ratio classes consistent with comparable assessments in Sweden (Länsstyrelsen Stockholm, 2025; Göteborg Kretslopp och Vatten, 2021b). A lower exposure threshold of 25% is applied based on findings that individual flood cells often occur adjacent to buildings and that such isolated flooding is unlikely to represent actual building flooding (Kretslopp och Vatten, 2021b).

Agricultural buildings, accessory buildings, and other minor buildings were excluded from the analysis because they are considered less relevant due to their limited size or low frequency of human use.

Table 2. Risk classification matrix for buildings based on building exposure ratio and maximum flood depth.

Max flood depth / **Building exposure**	0.1 – 0.3 m	0.3 – 0.5 m	> 0.5 m
25 – 50 %			
50 – 75 %			
> 75 %			

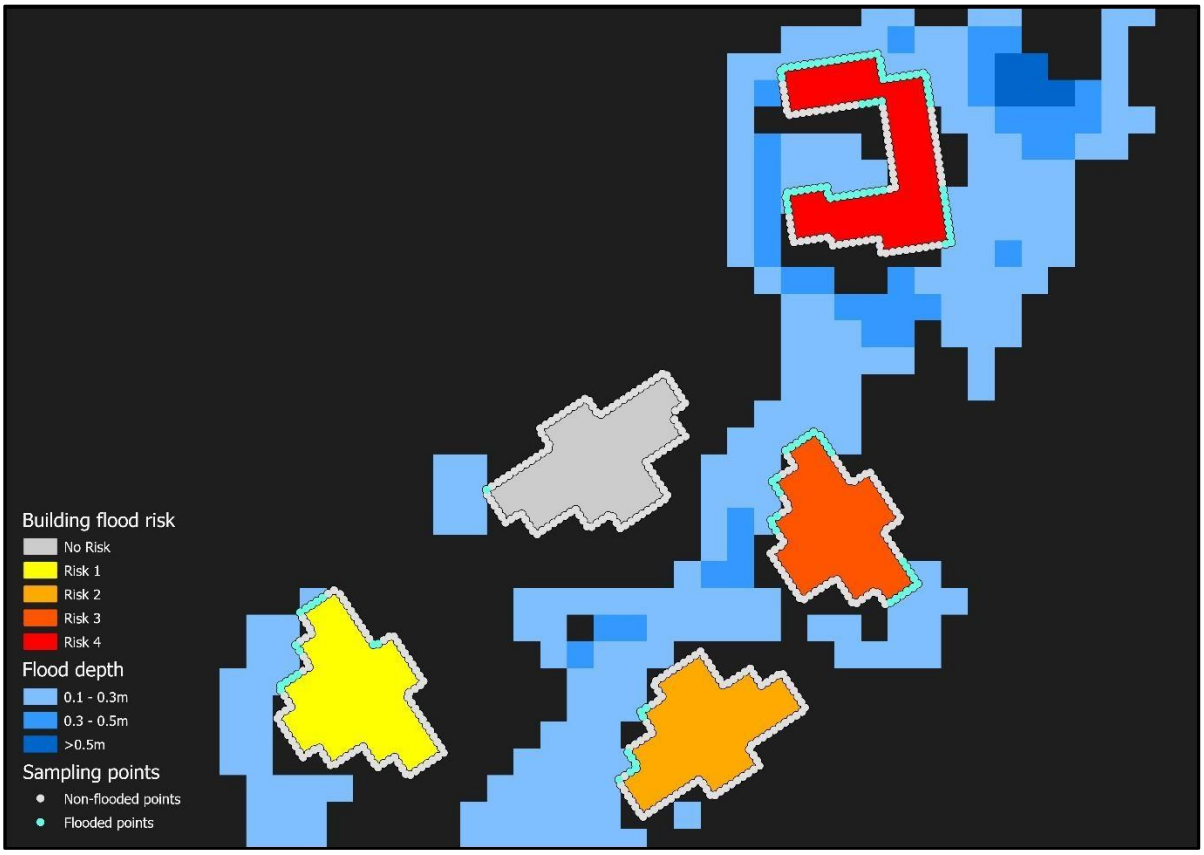

Figure 4. Illustration of the building flood risk methodology based on flood depth and building exposure.

City-scale building aggregation

To represent building flood risk at the city scale, individual building footprints were aggregated into a 1000 m hexagonal grid for visualization purposes. A hexagonal grid was selected because it improves the visual representation of spatial patterns. Rectangular grids can create strong horizontal and vertical lines that may draw attention to the grid itself rather than the underlying data. In contrast, hexagons break up these lines, making spatial patterns easier to see while also highlighting gradual changes and reducing visual bias caused by grid orientation (Esri, n.d.-b). To ensure meaningful representation, each hexagon was assigned the most prevailing risk class (1–4), given that it included at least 20 buildings with some type of risk. This threshold was chosen to balance spatial resolution and statistical robustness, ensuring that each hexagon reflects a sufficiently large building sample. Hexagons not meeting this criterion were visualized as No Risk.

Local-scale building case studies

The two hexagons with the highest proportion of Risk-4 buildings from the city-scale analysis were selected for local-scale analysis, given that they also met the following conditions: at least

30 Risk-4 buildings and a total building footprint across all classes covering more than 15% of the hexagon area. This ensured that the selected areas represented dense urban environments.

3.2.3 Combined flood risk evaluation

This evaluation integrates road inaccessibility and building flood risk to identify areas of overall high flood impact at the city scale. The components were combined using a weighted summation approach, a commonly applied decision rule in GIS-based multi-criteria analysis (Malczewski, 2006).

To enable integration, the previously identified inaccessible areas were summarized within each hexagon so that inaccessibility risk could be analysed in the same spatial format as building risk, allowing the two components to be combined into a single measure of overall risk. Inaccessible areas were classified into five classes based on total length of inaccessible roads within each hexagon: The classes are None (<200 m), Low (200 – 500 m), Moderate (500 – 2500 m), High (2500 – 4000 m), and Extreme (>4000 m). These thresholds were defined according to the study's minimum inaccessibility criterion (200 m) and the empirical distribution of the data, using the P75 (≈517 m), P90 (≈2530 m), and P95 (≈4034 m) percentiles to account for skewness and outliers.

The five inaccessibility classes were combined with the five building-risk classes to create a combined risk classification matrix (Table 3). Both components were converted to numerical scores (0–4), with inaccessibility given a weight of 0.4 and building risk a weight of 0.6 to emphasize human exposure. The weighting reflects an assumption of higher societal impact from building exposure; however, it should be interpreted as a simplified representation rather than an empirically validated weighting scheme. The resulting weighted scores were rounded to produce a final combined risk score, where higher values indicate higher combined risk.

Table 3. Combined risk classification matrix for road inaccessibility and building flood risk.

Inaccessibility / **Building risk**	None (0)	Low (1)	Moderate (2)	High (3)	Very high (4)
None (0)	0	0.4	0.8	1.2	1.6
None (0)	0	0.4	0.8	1.2	1.6
Low (1)	0.6	1	1.4	1.8	2.2
Moderate (2)	1.2	1.6	2	2.4	2.8
High (3)	1.8	2.2	2.6	3	3.4
Very high (4)	2.4	2.8	3.2	3.6	4

4 Results

The results are presented at two spatial scales: (1) a city scale, showing the overall spatial distribution of road inaccessibility, building flood risk, and their combined risk across Gothenburg, and (2) a local scale, focusing on detailed analyses of selected case study areas.

4.1 Road inaccessibility in Gothenburg

The results show that the majority of inaccessible areas are concentrated in the southwestern part of the study area, with the largest and most critical inaccessibility occurring in Torslanda and Näset (Figure 5). Areas with dense and well-connected road networks, such as the central areas of Gothenburg, maintain accessibility even under severe flooding, whereas peripheral areas with limited alternative routes experience higher levels of road inaccessibility. Smaller areas with lower levels of road inaccessibility are dispersed across the study area. Overall, 474.5 km of roads are located within areas classified as inaccessible in Gothenburg.

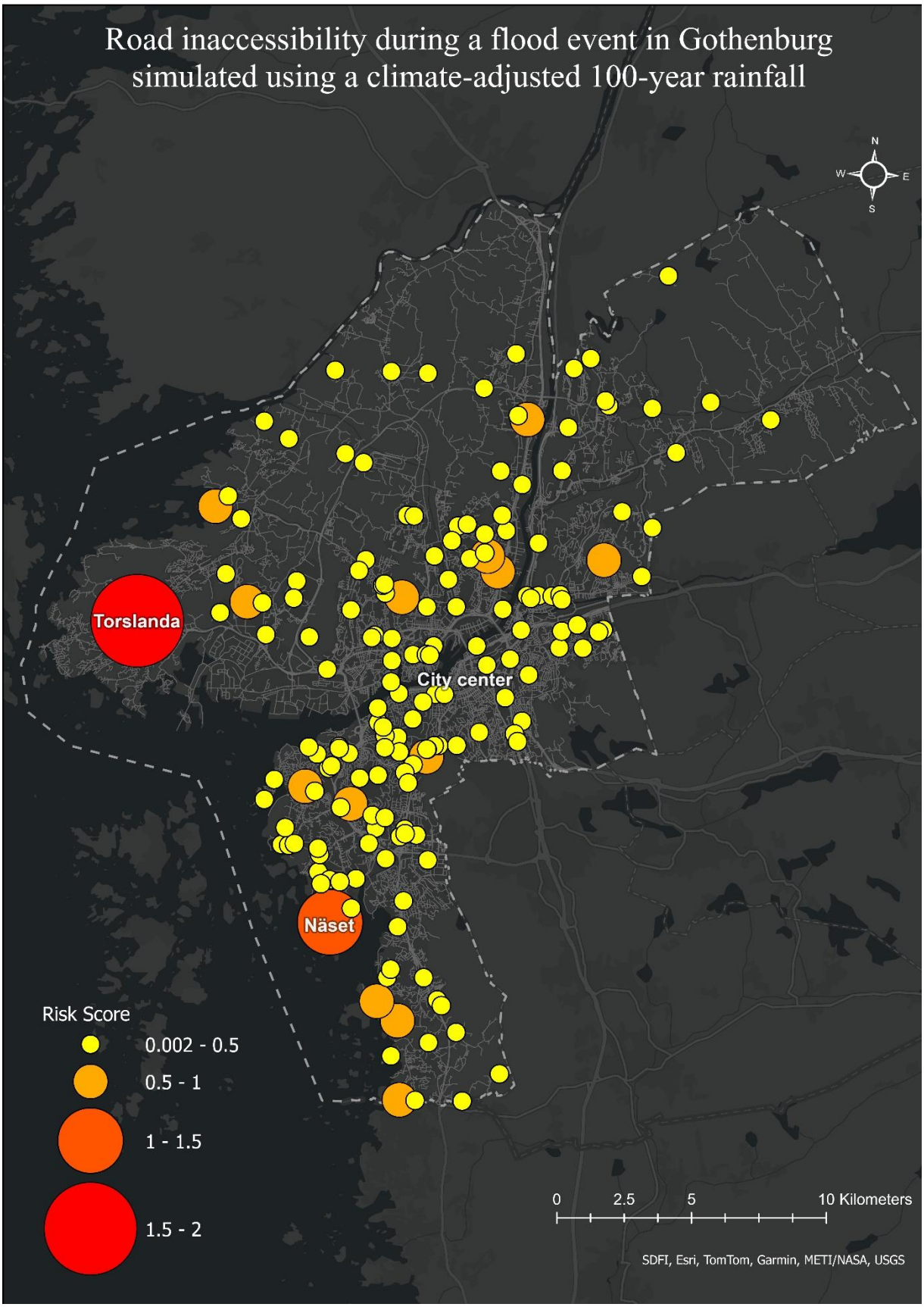

Figure 5. Spatial distribution of road inaccessibility in Gothenburg simulated using a climate-adjusted 100-year rainfall event, represented by graduated centroids weighted by a combined risk score derived from road length and building count (see Section 3.2.1).

4.2 Road inaccessibility – case studies

4.2.1 Näset

In the first case study, nearly the entire road network becomes inaccessible once the first flood barrier is encountered (Figure 6). Only a small number of road segments are affected by two or three flood barriers. This pattern is also reflected in Figure 7, which shows that 24.7 km of the road network is affected by one flood barrier compared to 1.1 km and 0.2 km affected by two and three flood barriers respectively. This indicates a highly centralized vulnerability structure, where targeted mitigation measures at a single critical point could substantially improve overall accessibility.

Figure 6. Spatial patterns of road inaccessibility in Näset simulated using a climate-adjusted 100-year rainfall event.

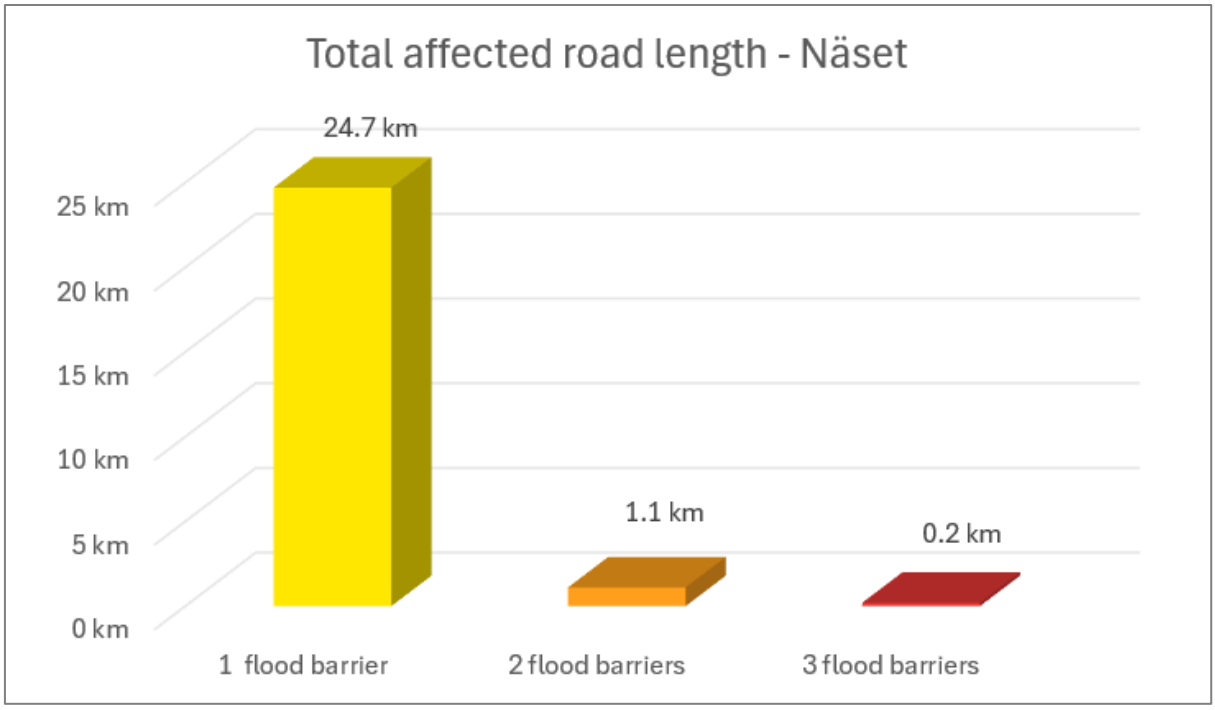

Figure 7. Total affected road length by number of flood barriers in Näset simulated using a climate-adjusted 100-year rainfall event.

4.2.2 Torslanda

In the second case study, two initial flood barriers cause road inaccessibility within the study area, one located in the northeast and one in the east (Figure 8). In total, seven flood barriers affect road accessibility in Torslanda when considering the shortest possible route from any of the initial barriers. This distributed vulnerability pattern indicates that multiple locations drive the network's vulnerability, suggesting that mitigation measures would need interventions at several locations rather than a single critical point. The results further show that the first, third, and fifth flood barriers affect the largest proportions of the road network, corresponding to 41.7 km, 63.4 km, and 51.4 km of inaccessible roads respectively (Figure 9).

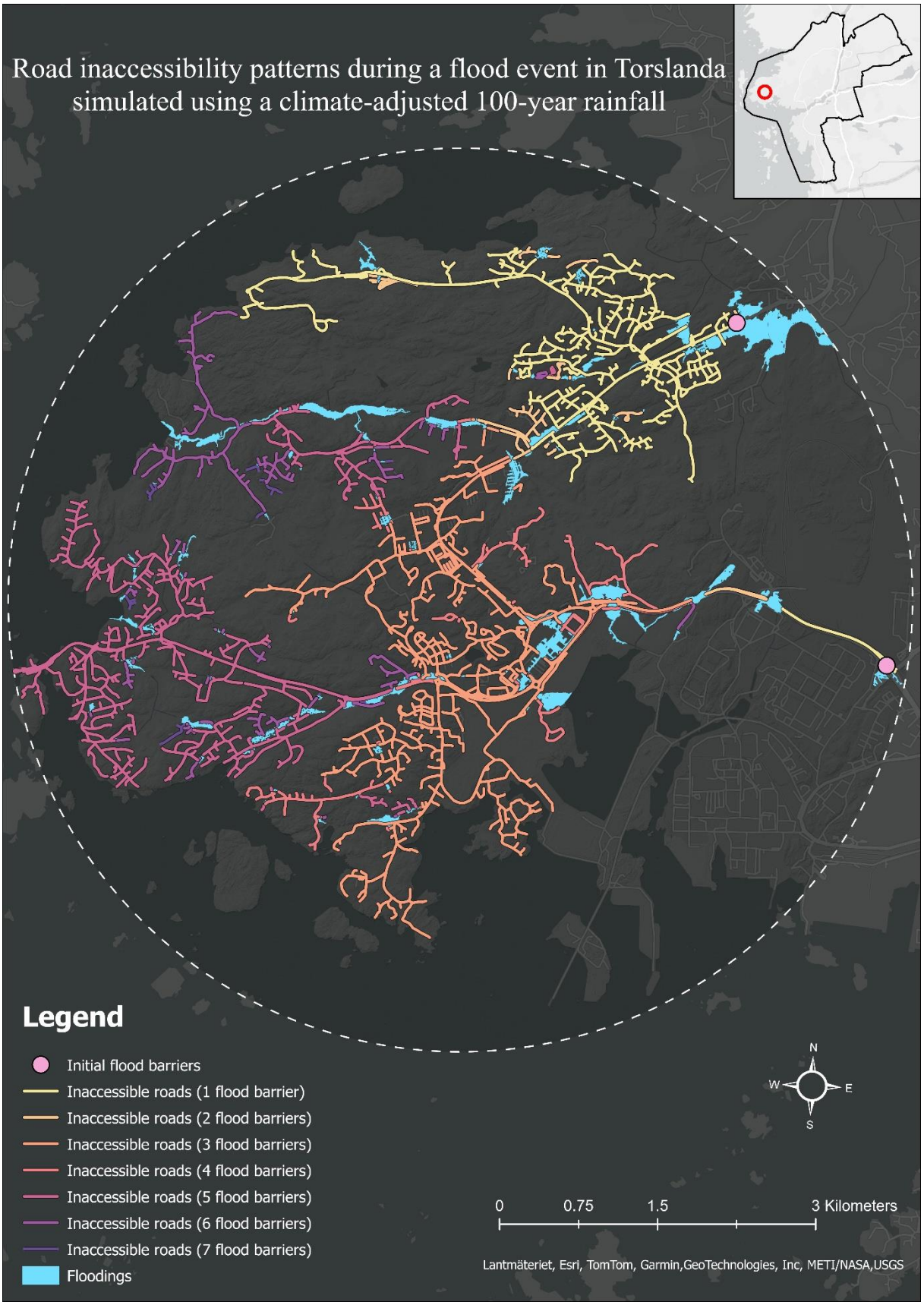

Figure 8. Spatial patterns of road inaccessibility in Torslanda simulated using a climate-adjusted 100-year rainfall event, classified by the minimum number of flood barriers crossed from either of the initial barriers.

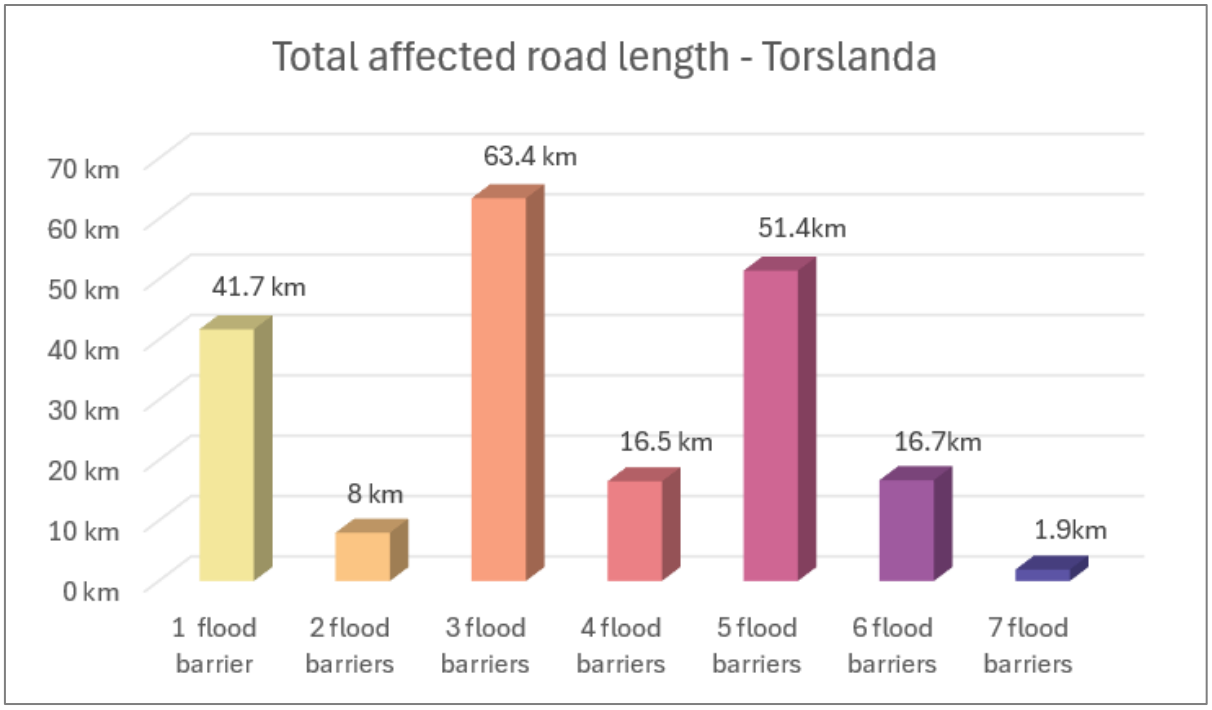

Figure 9. Total affected road length by number of flood barriers in Torslanda simulated using a climate-adjusted 100-year rainfall event.

4.3 Building flood risk in Gothenburg

The results identify four small clusters of areas with high building flood risk (Risk 4) located in Bergsjön, Gamlestaden, Kärrdalen, and Påvelund (Figure 10). Additional high-risk areas (Risk 4) are primarily found in the western part of the study area, while a large continuous area of relatively high building flood risk (Risk 3–4) is located southwest of the city center. Across the study area, 3.7% of the buildings belong to the highest risk class (Risk 4), while 9.2% fall within the two highest risk classes (Risk 3–4). Areas with no or low building flood risk are mainly found toward the outskirts of the study area. These areas are generally characterized by less intensive urban development, with higher surface permeability and in many cases higher elevation.

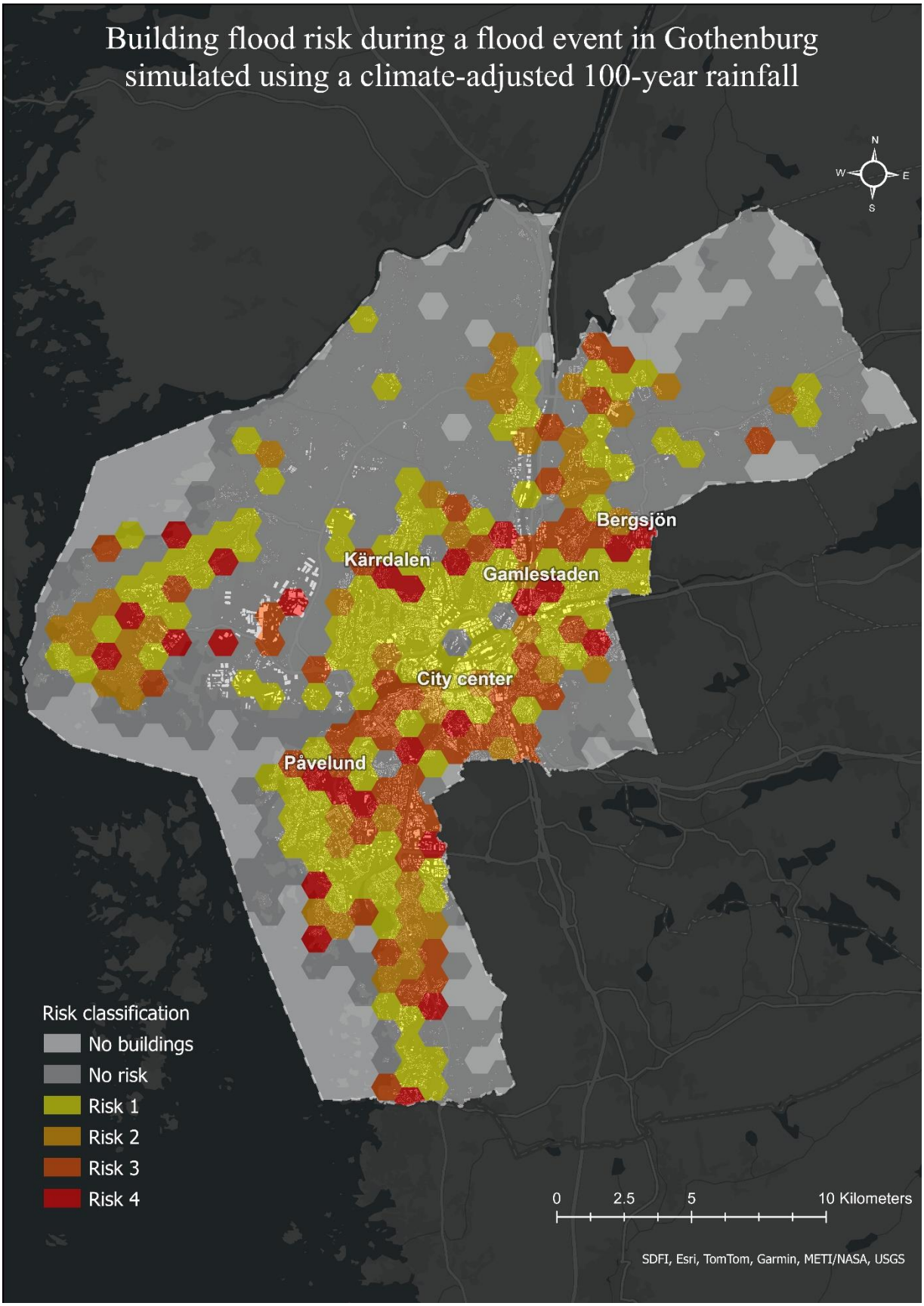

Figure 10. Spatial distribution of building flood risk in Gothenburg within a 1000 m hexagonal grid simulated using a climate-adjusted 100-year rainfall event.

4.4 Building flood risk – case studies

4.4.1 Gamlestaden

In the first case study, 16% of the buildings in Gamlestaden belong to the highest risk class (Risk 4). The industrial area along the railway in the central part of the study area exhibits the highest building flood risk, together with parts of the eastern residential area (Figure 11). This indicate that flood exposure is associated with land-use types characterized by high proportions of impermeable surfaces.

The central and western parts of the study area are dominated by industrial buildings, while the eastern part consists primarily of residential buildings. In addition, a school is identified among the buildings with relatively high building flood risk (Risk 3), indicating potential impact on essential services within the area.

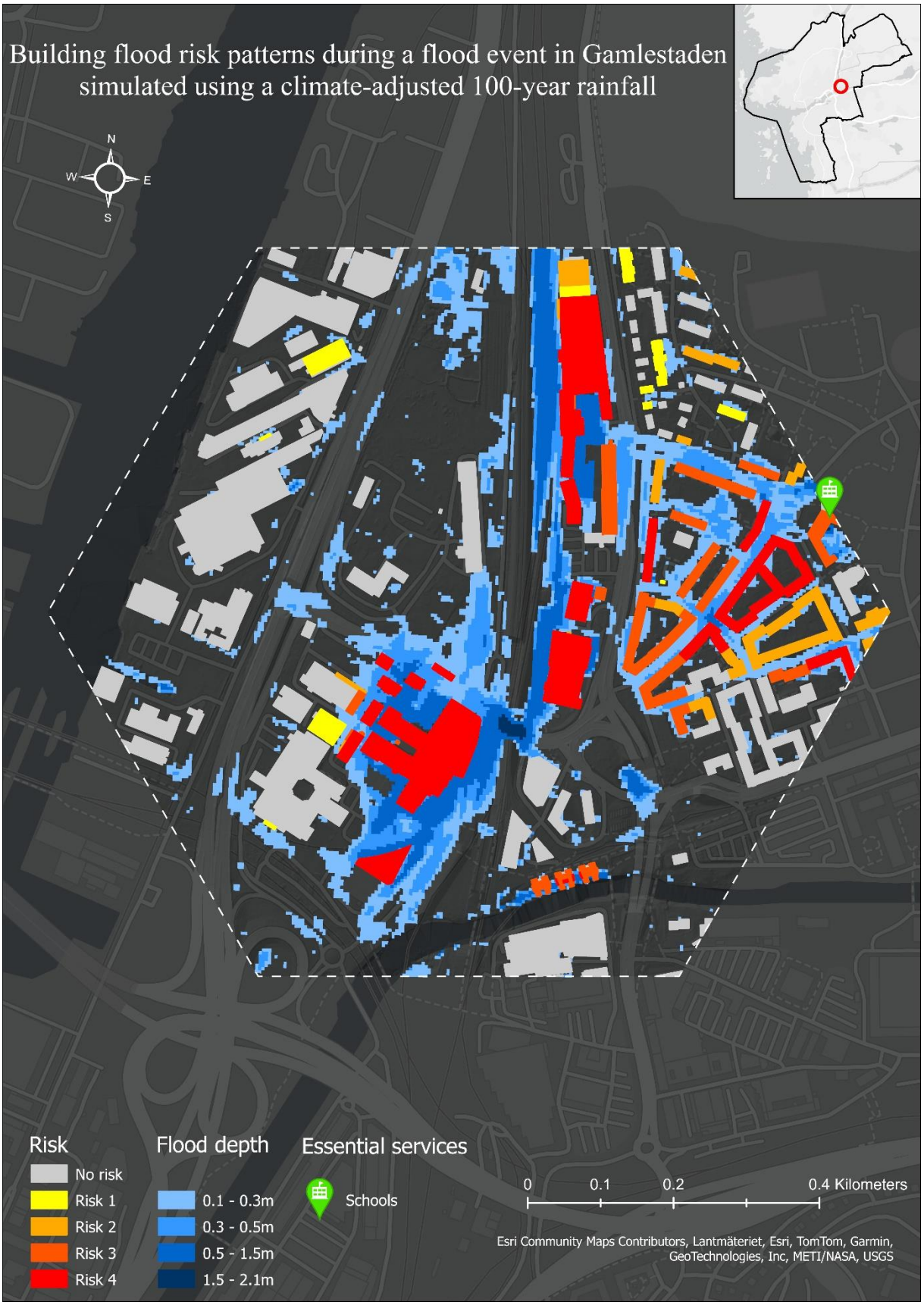

Figure 11. Spatial patterns of building flood risk in Gamlestaden simulated using a climate-adjusted 100-year rainfall event.

4.4.2 Björkekärr

In the second case study, 6.8% of the buildings in Björkekärr belong to the highest risk class (Risk 4). The northern low-lying areas are more severely affected than the southern more elevated areas which benefit from natural topographic protection (Figure 12). This contrast illustrates that even relatively small differences in elevation within urban neighbourhoods can strongly influence exposure to flooding.

A substantial portion of the high-risk buildings are large in size and includes essential services. The north-eastern part of the study area is dominated by healthcare facilities, while the remaining areas are characterized by residential buildings. The presence of healthcare facilities highlights the potential societal implications of flooding, as damage to essential services may have consequences that extend beyond direct physical damage to buildings.

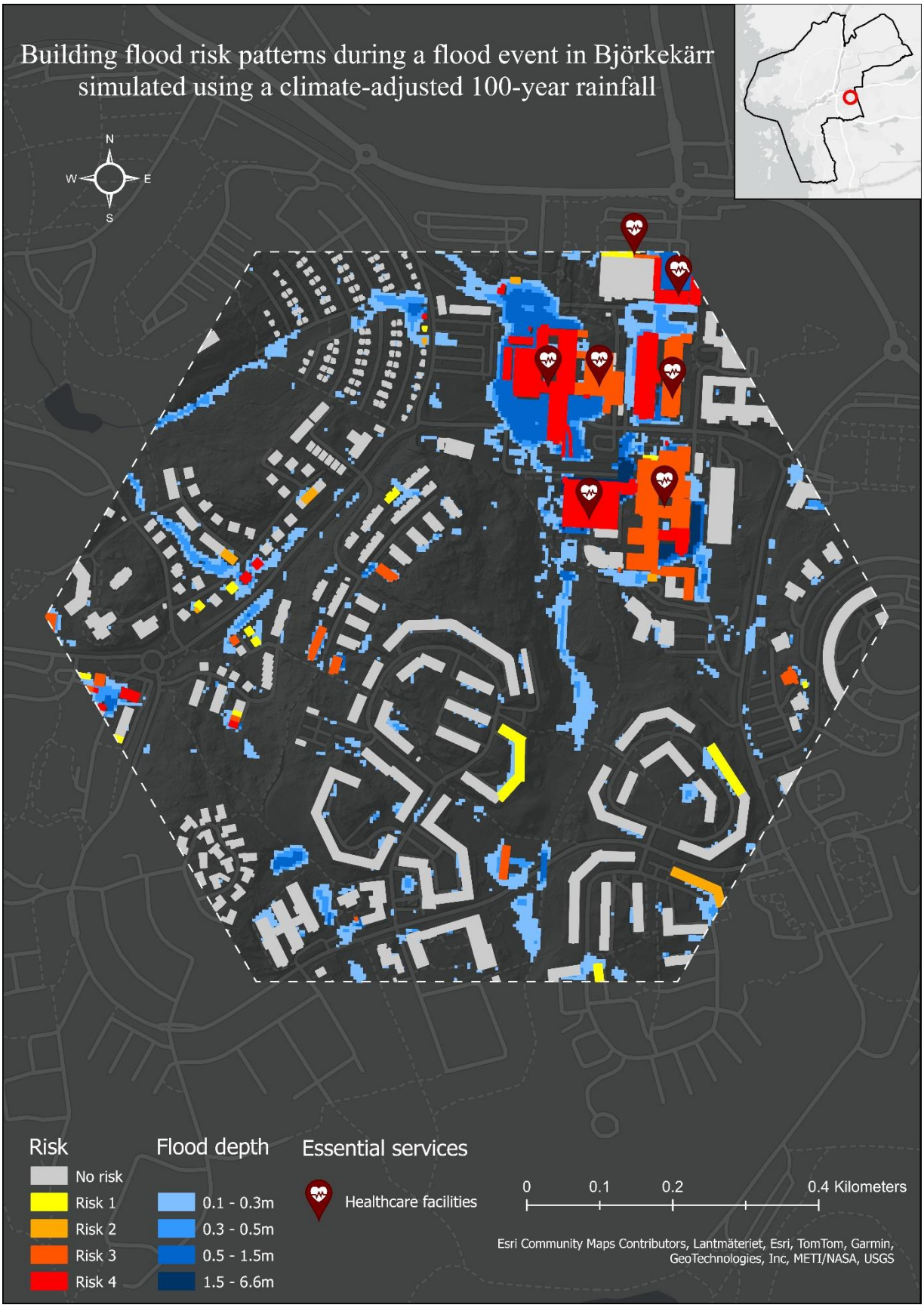

Figure 12. Spatial patterns of building flood risk in Björkekärr simulated using a climate-adjusted 100-year rainfall event.

4.5 Combined road inaccessibility and building flood risk in Gothenburg

The combined results identify areas expected to experience the highest overall impacts during a 100-year rainfall event, considering both road inaccessibility and building flood risk. Areas classified as Very High risk are limited in extent and occur mostly as single cells in the western part of the study area, whereas larger and more continuous clusters of High to Very High risk are identified in Backa, Torslanda, the industrial area of Volvo Cars, and the urban areas around Högsbo (Figure 13). In contrast, the outskirts of the study area are predominantly classified as Low risk or None.

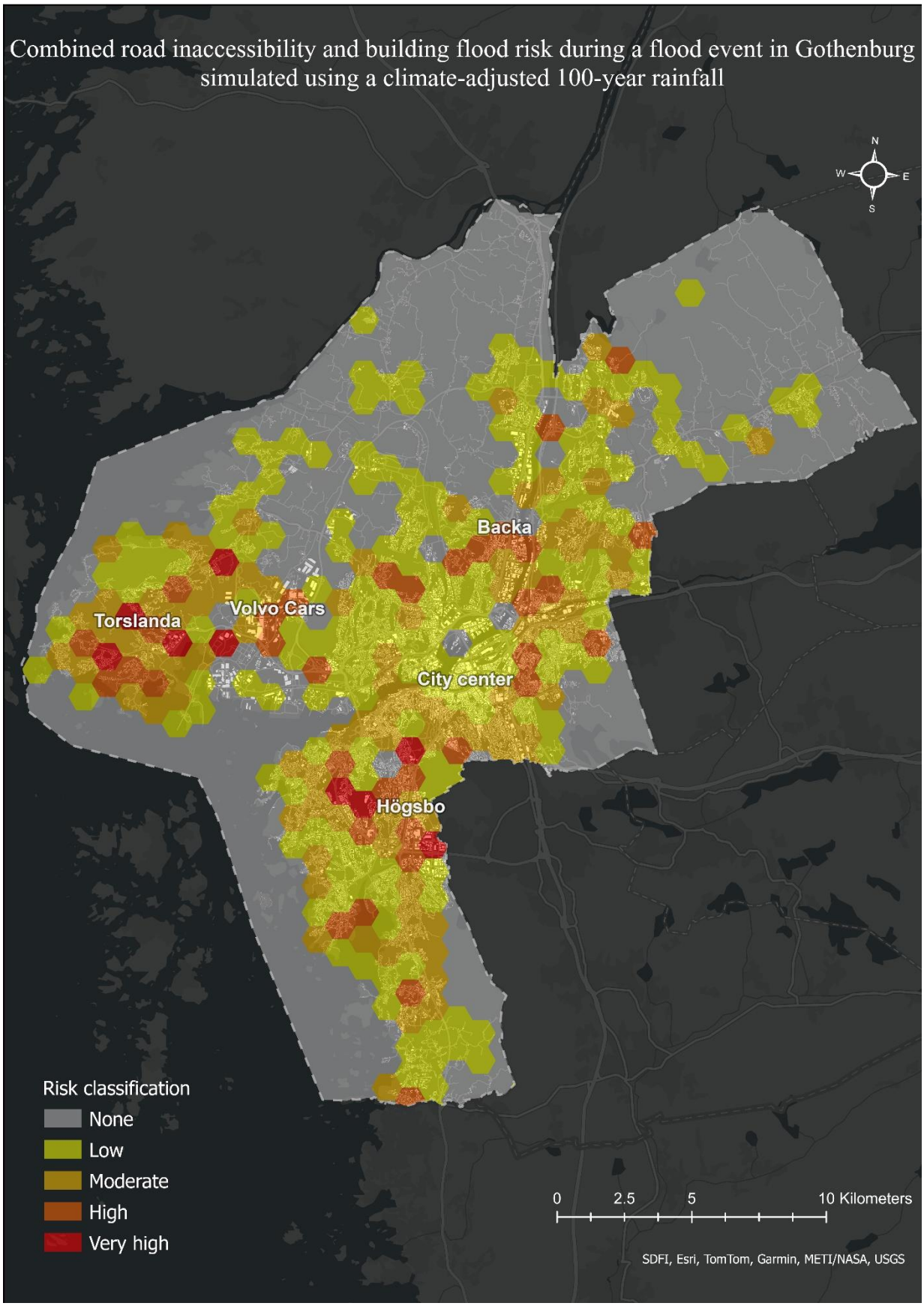

Figure 13. Spatial distribution of combined road inaccessibility and building flood risk in Gothenburg within a 1000 m hexagonal grid simulated using a climate-adjusted 100-year rainfall event.

5 Discussion

This section discusses the study's results and situates the findings in relation to previous urban flood research, reflects on methodological considerations, and provides suggestions for further research.

5.1 Interpretation of spatial patterns and the combined flood risk perspective

5.1.1 Road inaccessibility patterns

The results in this study show that road inaccessibility in Gothenburg is largely governed by network structure and connectivity, in combination with the spatial extent of the flooding. Peripheral areas with limited alternative routes, such as Torslanda and Näset, are particularly vulnerable, as localized flooding can disconnect large portions of the road network. These findings are consistent with previous research showing that network topology and connectivity are key determinants of flood-related accessibility loss. For example, Zhou et al. (2022) found that more than 40% of overall road connectivity was lost during a 100-year rainfall event at the city scale, even though flooding affected only limited parts of the road network. Similarly, He et al. (2022) conducted a global assessment of flood impacts on urban road networks and demonstrated that while only around 15% of road segments may be directly flooded during a 100-year rainfall event, nearly 45% of the simulated trips failed due to connectivity loss. Together, these findings suggest that even small-scale flooding can trigger system-wide accessibility disruptions, due to the network's limited redundancy.

The identified inaccessibility patterns have important practical implications. Reduced connectivity in peripheral areas such as Torslanda and Näset may limit access to critical facilities, including hospitals, fire stations and other emergency services, which can delay response times and complicate evacuation and recovery efforts. Previous studies have shown that flood-induced road closures can severely disrupt emergency access (Tsang & Scott, 2020; Coles et al., 2017).

5.1.2 Building flood risk patterns

The results in this study show that building flood risk in Gothenburg is strongly influenced by local topography and land-use patterns, with low-lying and industrial areas experiencing the highest exposure as illustrated by the case studies in Gamlestaden and Björkekärr. These patterns are consistent with previous research: Torgersen et al. (2017) found that buildings located in low-lying areas with concave topography are significantly more exposed to flooding, as such areas tend to accumulate surface runoff during extreme precipitation events. Land use

also plays a critical role in shaping flood risk, and Kaspersen et al. (2017) showed that pluvial flooding in urban areas can increase by up to 10% for every 1% increase in impervious surfaces. Considering that industrial areas are largely characterized by impervious surfaces, they are especially vulnerable to flood impacts. Together, these studies emphasize how both topography and land use shape spatial patterns of building flood risk.

Importantly, the results in this study represent relative building flood risk, reflecting spatial differences in exposure rather than absolute damage potential. Factors such as building construction material (Komolafe et al., 2016), basement presence (Tai et al. 2025), and ground-floor elevation (Diaz et al., 2024) are not explicitly accounted for in this analysis but would strongly influence actual flood impact.

5.1.3 Combined flood risk perspective

The combined flood risk evaluation in this study integrates building flood risk and road inaccessibility to identify areas where both structural exposure of buildings and functional disruptions of the road network coincide. This combined perspective provides insights that cannot be obtained from either component alone. While building flood risk reflects potential physical damage, road inaccessibility captures the loss of functional connectivity that restricts emergency response, evacuation, and post-event recovery. Zang et al. (2024) showed that floods do not affect buildings and roads in isolation but rather reshapes the whole urban system. By modelling buildings, roads and emergency facilities as a single compound network, they found that flood-induced road interruptions can reduce emergency accessibility once a collapse threshold in road capacity is reached. Because roads act as “bridges” between buildings and emergency services, changes in road accessibility dynamically redistribute the building flood risk and recovery capacity over time, especially in residential and commercial areas (Zang et al., 2024).

This supports the need for a combined flood risk perspective as assessing only building flood risk or road inaccessibility would miss these dynamic interaction effects. By integrating building-level risk with network-based accessibility loss, the combined perspective helps identify areas where flood events are likely to generate the greatest societal consequences. This integrated approach supports more informed decision-making for urban resilience planning and emergency preparedness.

5.2 Method discussion

5.2.1 Data and limitations of the 100-year flood raster

The 100-year flood raster is derived from hydrodynamic simulations that incorporate elevation, land use, soil types, rainfall, and sewer systems to simulate urban flood conditions. Among these inputs, elevation data is particularly influential in determining surface flow paths and water accumulation patterns, while land use and soil properties govern infiltration processes, which are widely recognised as a major source of uncertainty in urban flood modelling (Kazma & Taha, 2026). Both the elevation data and the land use data reflect conditions at the time of the data acquisition in 2017, when the height scanning and land-use mapping were conducted. Consequently, areas where significant changes to terrain or urban structure have occurred since then may not be accurately represented, and results for such areas should therefore be interpreted with caution.

As with all hydrological modelling approaches, some uncertainty arises from simplified representations of physical processes, which may influence the simulated flood patterns represented in the raster. Nevertheless, the modelling framework on which the raster is based follows a physically-based approach that captures the dominant processes controlling urban flooding, supporting its overall validity. Direct validation of flood simulations for extreme precipitation events is challenging due to the rarity of such events and the limited availability of observational data. The modelling methodology has however previously been evaluated in Malmö for a 300-year rainfall event using observed precipitation data, and as the same methodology is applied here, the flood raster for Gothenburg can therefore be considered indirectly validated (Göteborg Kretslopp och Vatten, 2021a).

The flood raster has a 4 x 4 m spatial resolution, balancing sufficient detail for most urban structures with reasonable computation times. While well suited for identifying broader spatial patterns, the resolution limits the representation of fine-scale urban features, which introduces greater uncertainty in highly detailed analyses.

5.2.2 Network-based service area analysis of road inaccessibility

The selection of flood thresholds strongly shapes the service area analyses of road inaccessibility. A flood depth threshold of 30 cm is widely recognized as critical for safe driving of most passenger cars, balancing safety and practical considerations, though tolerance varies by vehicle type (Pregnolato, 2017). That threshold is used in this study and is commonly used in other accessibility analyses under flood conditions (Li et al., 2018; Suwanno et al., 2023),

while different inundation thresholds may be applied for vehicle-specific analyses (Abdulla et al., 2020). The minimum flood extent and size thresholds in this study (10 meters and 500 m²) are used to filter out noise and ensure meaningful disruptions, reflecting the assumption that larger simulated flooding is more likely to result in actual flooding. The thresholds should be considered carefully when interpreting the results, as alternative thresholds can lead to substantially different outcomes. In addition, while a 2000-meter buffer was applied to the road network to reduce edge effects, flood data was limited to the municipal boundary, potentially underestimating impacts on roads near the edges of the study area.

The treatment of bridges introduces further uncertainty. A 20-meter buffer around bridge endpoints was applied to avoid false flooding caused by the combination of short bridge segments and the flood raster resolution (4 x 4 m), however, bridge approaches can also be critical flood points, which are not captured in this study. Smaller bridges not included in the dataset were identified by intersecting flooded roads with watercourses, assuming that any road crossing a watercourse corresponds to a bridge structure, which is reasonable in many cases but not universally true. An alternative approach to assessing bridge flood risk could be to identify the elevation differences between bridge structures and the water surface, classifying bridges within 1 meter of the water level as inaccessible, following Papilloud et al. (2024).

Finally, the criteria used to define inaccessible areas – requiring a minimum of 200 meters continuous inaccessible road and at least 5 buildings within 50 meters – helps to ensure that the identified areas represent a meaningful amount of inaccessibility. However, this threshold may exclude small disruptions with local relevance.

5.2.3 Building flood risk analysis

A challenge in the building flood risk analysis is that the buildings themselves typically not include flood information, and flood data is not always available precisely at the building locations. To address this, building footprints were buffered by 4 meters, allowing extraction of flood depth values from the 100-year flood raster while minimizing overlap with neighbouring buildings. A similar approach has been used by Bertsch et al. (2022), who applied buffers of 1.5 to 4 meters to assign flood depth values to building footprints. Despite this, some uncertainty remains, especially in densely built urban areas where buildings are closely spaced.

The classification matrix (Table 2) used to derive building flood risk plays a central role in shaping the results. By combining flood depth and building exposure, the matrix provides a more nuanced understanding of building-level risk. Although the selected components and class

intervals align with other Swedish building flood risk studies (DHI, 2014; Structor, 2017; WSP, 2023, Länsstyrelsen Stockholm, 2025; Göteborg Kretslopp och Vatten, 2021b), alternative thresholds could produce different spatial patterns, highlighting the interpretative nature of risk classifications.

At the city scale, the chosen aggregation threshold influences how risk patterns are visualized and interpreted. To ensure meaningful representation, each hexagon was assigned the most prevailing risk class (1–4), provided that it included at least 20 buildings with some type of risk. This approach captures the dominant risk class while maintaining a sufficient sample size, although it may underrepresent areas where multiple risk classes show high prevalence and areas with few but vulnerable buildings. This trade-off highlights a fundamental challenge in spatial aggregation, balancing sensitivity with interpretability.

5.2.4 Combined flood risk evaluation

The combined flood risk evaluation in this study builds on both the building flood risk and road inaccessibility analyses and is structured around a classification matrix where inaccessibility was given a weight of 0.4 and building risk a weight of 0.6 to emphasize human exposure. Additional factors such as building type, road type, and essential services, could be incorporated to provide a more nuanced assessment of the actual risk level. These factors could for instance be integrated using advanced Multi-Criteria Decision Methods (MCDM) such as Analytical Hierarchy Process (AHP) and Technique for Order Preference by Similarity to Ideal Solution (TOPSIS), which are widely used for flood risk assessments in order to systematically incorporate and weight multiple risk factors (Pathan et al., 2022; Gosh & Kar, 2018; Mitra et al., 2023)

In addition, the criteria used to classify building flood risk and inaccessibility risk play a central role in defining which areas that are considered severely affected. Since inaccessibility was not analysed in the same spatial format as buildings, a classification of inaccessibility within hexagons was required. The classification thresholds were defined according to the minimum criterion for road inaccessibility (200 m) and the 75^{th}, 90^{th} and 95^{th} percentiles. While this is reasonable for the dataset used in this study, inaccessibility risk classes should ideally be standardized by absolute length or area, independent of data distribution. However, no "universal" classification scheme for road inaccessibility was found in the literature.

5.3 Further research

Future research could extend this work in several directions. Incorporating multiple rainfall scenarios with both shorter and longer return periods would help assess the robustness of the results. Testing alternative flood thresholds for both road inaccessibility and building flood risk would provide valuable insight into how varying inundation depths influence estimated flood impacts. Future research should also investigate the role of flood duration and water velocity, as these factors can strongly influence both traffic disruptions and building damage. In addition, using an updated flood model with higher spatial resolution could improve the representation of recent urban development and fine-scale flood dynamics.

Future accessibility analyses could be expanded to include travel-time analyses, enabling estimation of how much travel time increases during extreme precipitation events. Assessing accessibility and travel times to critical facilities such as hospitals, fire stations, and other emergency services would provide valuable operational insight for emergency response and urban resilience planning.

Building flood risk analyses would benefit from incorporating additional vulnerability indicators such as construction materials, basement presence, and ground-floor elevation, enabling a more comprehensive representation of flood impacts. Further work could also focus on specific building types, for example evaluating the exposure of essential services or identifying which building categories are most affected by flooding.

Finally, detailed case studies of areas identified as having high combined flood risk could provide deeper insight into local conditions and support the identification of targeted mitigation and adaptation measures.

6 Conclusion

This study shows that urban flood impacts, as simulated for a climate-adjusted 100-year rainfall event in Gothenburg, are unevenly distributed and strongly shaped by urban structure, network connectivity, and topography. Road inaccessibility is most severe in peripheral areas with low network redundancy where limited alternative routes can lead to extensive accessibility loss, while the highest building flood risk is primarily concentrated in low-lying and industrial areas.

The findings further highlight the importance of scale in urban flood risk assessments. City-scale analyses are effective for identifying overall spatial patterns of flood risk, whereas local-scale analyses provide deeper insights into how flood impacts emerge and vary within specific areas. In this study, detailed case studies demonstrated how localized flooding can both disrupt road networks at vulnerable sections and generate uneven building-level risk, underscoring the added value of fine-scale assessments.

By integrating road inaccessibility with building flood risk, this study identifies areas where flooding is likely to generate the greatest societal consequences. The combined perspective captures both functional disruptions to urban accessibility and direct impacts on the built environment, revealing vulnerabilities that would not be apparent from either component alone. This reinforces the importance of integrated flood risk assessments to support strategic urban resilience planning.

7 References

Abdulla, B., Kiaghadi, A., Rifai, H.S., & Birgisson, B. (2020). Characterization of vulnerability of road networks to fluvial flooding using SIS network diffusion model. *Journal of Infrastructure Preservation and Resilience, 1*(6). https://doi.org/10.1186/s43065-020-00004-z

Alabbad, Y., Mount, J., Campbell, A.M., & Demir, I. (2024). A web-based decision support framework for optimizing road network accessibility and emergency facility allocation during flooding. *Urban Informatics, 3*(10). https://doi.org/10.1007/s44212-024-00040-0

Beck, H.E., McVicar, T.R., Vergopolan, N., Berg, A., Lutsko, N.J., Dufour, A., Zeng, Z., Jiang, X., van Dijk, A.I.J.M., & Miralles, D.G. (2023). High-resolution (1 km) Köppen-Geiger maps for 1901–2099 based on constrained CMIP6 projections. *Scientific Data, 10*(1), 724. https://doi.org/10.1038/s41597-023-02549-6

Bertsch, R., Glenis, V., & Kilsby, C. (2022). Building level flood exposure analysis using a hydrodynamic model. Environmental Modelling & Software, 156, 105490. https://doi.org/10.1016/j.envsoft.2022.105490

Coles, D., Yu, D., Wilby, R.L., Green, D., & Herring, Z. (2017). Beyond 'flood hotspots': Modelling emergency service accessibility during flooding in York, UK. *Journal of Hydrology, 546*, 419–436. https://doi.org/10.1016/j.jhydrol.2016.12.013

Danmarks Meteorologiske Institut [DMI]. (2011, July 4) *Skybrud over København*. Retrieved 2025-11-23 from https://www.dmi.dk/nyheder/2011/skybrud-over-kobenhavn

DHI. (2014). *Risk- och sårbarhetsanalys avseende klimatförändringars påverkan för tätorterna Borgholm och Köpingsvik*. Borgholms kommun. https://www.borgholm.se/wpcontent/uploads/2023/10/Bilaga-11.-Risk-och-sarbarhetsanalys-avseende-klimatforandringar-Borgholm-Kopingsvik-DHI-2014-04-30.pdf

Diaz, N.D., Lee, Y., Kothuis, B.L.M., Pagán-Trinidad, I., Jonkman, S.N., & Brody, S.D. (2024). Mapping the Flood Vulnerability of Residential Structures: Cases from The Netherlands, Puerto Rico, and the United States. *Geosciences, 14*(4), 109. https://doi.org/10.3390/geosciences14040109

Esri. (n.d.-a). *Service area analysis.* Retrieved 2025-11-23 from https://desktop.arcgis.com/en/arcmap/latest/extensions/network-analyst/service-area.htm

Esri. (n.d.-b). *Why hexagons?* Retrieved 2026-03-18 from https://pro.arcgis.com/en/pro-app/3.4/tool-reference/spatial-statistics/h-whyhexagons.htm

Gosh, A., & Kar S.K. (2018). Application of analytical hierarchy process (AHP) for flood risk assessment: A case study in Malda district of West Bengal, India. *Natural Hazards, 94*(1), 349–368. https://link-springer-com.ludwig.lub.lu.se/article/10.1007/s11069-018-3392-y

Göteborg Kretslopp och Vatten. (2021a, January). *Modelldokumentation av Strukturplansmodeller: Dokumentation av Skyfallsmodeller uppsatta 2020* (PDF). Vatten i Göteborg. https://www.vattenigoteborg.se/Downpour/DownpourReports

Göteborg Kretslopp och Vatten. (2021b, January). *Strukturplan för hantering av översvämningsrisker: Metodbeskrivning* (PDF). Vatten i Göteborg. https://www.vattenigoteborg.se/Downpour/DownpourReports

Göteborgs Stad. (n.d.-a). *Historiska skyfall i Göteborg*. Göteborgs Stad. Retrieved 2025-11-23 from https://goteborg.se/wps/portal/start/bygga-bo-och-leva-hallbart/vatten-ochavlopp/dagvatten-och-skyfall/goteborgs-skyfallssasong-2025/historiska-skyfall-i-goteborg

Göteborgs Stad. (n.d.-b). *Befolkningsprognos Göteborg 2025–2050*. Retrieved 2025-11-23 from https://goteborg-statistik-och-analys.quarto.pub/befolkningsprognos-2025-2050/

He, Y., Rentschler, J., Gao, J., Yue, X., Radke, J., & Avner, P. (2022). *Mobility and resilience: A global assessment of flood impacts on road transportation networks* (Policy Research Working Paper No. 10049). World Bank. https://doi.org/10.1596/1813-9450-10049

Huizinga, J., De Moel, H., & Szewczyk, W. (2017). *Global flood depth-damage functions: Methodology and the database with guidelines* (JRC105688). Publication Office of the European Union. https://doi.org/10.2760/16510

IPCC, 2023: Sections. In: Climate Change 2023: Synthesis Report. Contribution of Working Groups I, II and III to the Sixth Assessment Report of the Intergovernmental Panel on

Climate Change [Core Writing Team, H. Lee and J. Romero (eds.)]. IPCC, Geneva, Switzerland, pp. 35–115. https://doi.org/10.59327/IPCC/AR6-9789291691647

Kaspersen, P.S., Ravn, N.H., Arnbjerg-Nielsen, K., Madsen, H., & Drews, M. (2017). Comparison of the impacts of urban development and climate change on exposing European cities to pluvial flooding. *Hydrology and Earth System Sciences, 21*(8), 4131–4147. https://doi.org/10.5194/hess-21-4131-2017

Kazma, M.H., & Taha, A.F. (2026). *Exploring Uncertainty Propagation in Coupled Hydrologic and Hydrodynamic Systems via Distribution-Agnostic State Space Analysis.* arXiv. https://doi.org/10.48550/arXiv.2603.05740

Komolafe, A.A., Herath, S., & Avtar, R. (2019). Establishment of detailed loss functions for the urban flood risk assessment in Chao Phraya River basin, Thailand. *Geomatics, Natural Hazards and Risk, 10*(1), 633–650. https://doi.org/10.1080/19475705.2018.1539038

Lantmäteriet. (2024, October 18). *PRODUCT DESCRIPTION Topography 10 Download, vector.* https://www.lantmateriet.se/globalassets/geodata/geodataprodukter/e-pb-topografi-10nedladdning-vektor.pdf

Li, M., Kwan, M-P., Yin, J., Yu, D., & Wang, J. (2018). The potential effect of a 100-year pluvial flood event on metro accessibility and ridership: A case study of central Shanghai, China. *Applied Geography, 100*, 21–29. https://doi.org/10.1016/j.apgeog.2018.09.001

Lin, X., Lu, Q., Chen, L., & Brilakis, I. (2024). Assessing dynamic congestion risks of flood disrupted transportation network systems through time-variant topological analysis and traffic demand dynamics. *Advanced Engineering Informatics, 62*(Part A), 102672. https://doi.org/10.1016/j.aei.2024.102672

Länsstyrelsen Stockholm. (2025). Strukturplan för hantering av skyfallsrisker: KUNSKAPSSTÖD (Rapport 2025:8). https://www.lansstyrelsen.se/download/18.4c443e4619540d2095a1fc77/174100733187/R2025-08-Strukturplan%20f%C3%B6r%20skyfall%20-%20Kunskapsst%C3%B6d.pdf

Malczewski, J. (2006). GIS-based multicriteria decision analysis: a survey of the literature. *International Journal of Geographical Information Science, 20*(7), 703–726. https://doi.org/10.1080/13658810600661508

Mitra, R., Das, J., & Kamruzzaman, M. (2023). Application of TOPSIS method for flood susceptibility mapping using Excel and GIS. *MethodsX, 11*, 102263. https://doi.org/10.1016/j.mex.2023.102263

Myhre, G., Alterskjær, K., Stjern, C.W., Hodnebrog, Ø., Marelle, L., Samset, B.H., Sillmann, J., Schaller, N., Fischer, E., Schulz, M., & Stohl, A. (2019). Frequency of extreme precipitation increases extensively with event rareness under global warming. *Scientific Reports, 9,* 16063. https://doi.org/10.1038/s41598-019-52277-4

Myndigheten för samhällsskydd och beredskap [MSB]. (2016). *Skyfallsförebyggande åtgärder: Exempel från arbete i Köpenhamns och Fredriksbergs kommune*r (MSB1018). https://rib.msb.se/filer/pdf/28191.pdf

Myndigheten för samhällsskydd och beredskap [MSB]. (2017, August). *Vägledning för Skyfallskartering: Tips för genomförande och exempel på användning* (MSB1121). https://rib.msb.se/filer/pdf/28389.pdf

Myndigheten för samhällsskydd och beredskap [MSB]. (2020). *Förordningen om Översvämningsrisker – Sveriges genomförande av EU:s översvämningsdirektiv* (MSB1657). https://rib.msb.se/filer/pdf/29445.pdf

Nyberg, L., Hakkarainen, H., Blumenthal, B., & Moberg, J.-O. (2019). *Konsekvenser av sommarskyfall i Sverige under åren 2009–2018: Analys av rapportering i dagstidningar* (Rapport 2019:2). Centrum för klimat och säkerhet, Karlstads universitet. https://www.kau.se/files/2019-05/CCS_2019-2.pdf

Olsson, J., Berg, P., Erron, A., Simonsson, L., Södling, J. Wern, L., & Yang, W. (2017). *Extremregn i nuvarande och framtida klimat Analyser av observationer och framtidsscenarier* (Klimatologi Nr 47). Sveriges Meteorologiska och Hydrologiska Institut(SMHI).https://www.smhi.se/download/18.18f5a56618fc9f08e8329c85/1717801000450/Klimatologi_47%20Extremregn%20i%20nuvarande%20och%20framtida%20klimat%20Analyser%20av%20observationer%20och%20framtidsscenarier.pdf

Openshaw, S. (1984). *The modifiable areal unit problem* (Concepts and Techniques in Modern Geography No. 38). Geo Books.

Papilloud, T., Röthlisberger, V., Loreti, S., & Keiler, M. (2020). Flood exposure analysis of road infrastructure – Comparison of different methods at national level. *International*

Journal of Disaster Risk Reduction, 47, 101458. https://doi.org/10.1016/j.ijdrr.2020.101548

Papilloud, T., Steiner, A., Zischg, A., & Keiler, M. (2024). Road network disruptions during extreme flooding events and their impact on the access to emergency medical services: A spatiotemporal vulnerability analysis. *Science of the Total Environment, 956*, 177140. https://doi.org/10.1016/j.scitotenv.2024.177140

Pathan, A.I., Agnihotri, P.G., Said, S., & Patel, D. (2022). AHP and TOPSIS based flood risk assessment: A case study of the Navsari City, Gujarat, India. *Environmental Monitoring and Assessment, 194*(7), 509. https://doi.org/10.1007/s10661-022-10111-x

Paulik, R., Zorn, C., Wotherspoon, L., & Sturman, J. (2023). Modelling national residential building exposure to flooding hazards. *International Journal of Disaster Risk Reduction, 94,* 103826. https://doi.org/10.1016/j.ijdrr.2023.103826

Pregnolato, M., Ford, A., Wilkinson, S.M., & Dawson, R.J. (2017). The impact of flooding on road transport: A depth-disruption function. *Transportation Research Part D: Transport and Environment, 55*, 67–81. https://doi.org/10.1016/j.trd.2017.06.020

Schimanke, S., Joelsson, M., Andersson, S., Carlund, T., Wern, L., Hellström, S., & Kjellström, E. (2022). *Observerad klimatförändring i Sverige 1860–2021* (Klimatologi Nr 69). Sveriges Meteorologiska och Hydrologiska Institut (SMHI).https://www.smhi.se/download/18.18f5a56618fc9f08e832cbc3/1717804715501/Klimatologi_69%20Observerad%20klimatf%C3%B6r%C3%A4ndring%20i%20Sverige%2018602021.pdf

Seneviratne, S.I., X. Zhang, M. Adnan, W. Badi, C. Dereczynski, A. Di Luca, S. Ghosh, I. Iskandar, J. Kossin, S. Lewis, F. Otto, I. Pinto, M. Satoh, S.M. Vicente-Serrano, M. Wehner, and B. Zhou, 2021: Weather and Climate Extreme Events in a Changing Climate. In Climate Change 2021: The Physical Science Basis. Contribution of Working Group I to the Sixth Assessment Report of the Intergovernmental Panel on Climate Change [Masson-Delmotte, V., P. Zhai, A. Pirani, S.L. Connors, C. Péan, S. Berger, N. Caud, Y. Chen, L. Goldfarb, M.I. Gomis, M. Huang, K. Leitzell, E. Lonnoy, J.B.R. Matthews, T.K. Maycock, T. Waterfield, O. Yelekçi, R. Yu, and B. Zhou (eds.)]. Cambridge University Press, Cambridge, United Kingdom and New York, NY, USA, pp. 1513–1766. https://doi.org/10.1017/9781009157896.013

Sjökvist, E., Andersson, M., Eklund, A., Karlsson, E., & Norman, M. (2025). *Klimatunderlag för klimat- och sårbarhetsanalyser* (Klimatologi Nr 74). Sveriges Meteorologiska och Hydrologiska Institut (SMHI). https://klimatanpassningsradet.se/download/18.53cdce23194f389da05422f/1740560511813/K limatologi_74%20Klimatunderlag%20f%C3%B6r%20klimat-%20och%20s%C3%A5rbarhetsanalyser.pdf

Statistiska centralbyrån [SCB]. (2025, February 21). *Folkmängd, topp 50, 31 december 2024.* Retrieved 2025-11-23 from https://www.scb.se/hitta-statistik/statistik-efter-amne/befolkningoch-levnadsforhallanden/befolkningens-sammansattning-ochutveckling/befolkningsstatistik/pong/tabell-och-diagram/folkmangd-ochbefolkningsforandringar---helarsstatistik/folkmangd-topp-50/

Structor. (2017). *Klimat - och sårbarhetsanalys. Byggnaders utsatthet för översvämning och försämrad markstabilitet. Fastighetskontoret i Stockholms stad.* Stockholms Stad. https://miljobarometern.stockholm.se/content/docs/tema/klimat/klimatanpassning/Klimat-ochs%C3%A5rbarhetsanalys-Fastighetskontoret-2017.pdf

Suwanno, P., Yaibok, C., Tsumita, N., Fukuda, A., Theerathitichaipa, K., Seefong, M., Jomnonkwao, S., & Kasemsri, R. (2023). Estimation of the Evacuation Time According to Different Flood Depths. *Sustainability, 15*(7), 6305. https://doi.org/10.3390/su15076305

Sveriges Meteorologiska och Hydrologiska Institut (SMHI). (n.d.-a). *Sveriges klimat*. SMHI. Retrieved 2025-11-23 from https://www.smhi.se/kunskapsbanken/klimat/sveriges-klimat

Sveriges Meteorologiska och Hydrologiska Institut (SMHI). (n.d.-b). *Hur var vädret: Göteborg*. SMHI. Retrieved 2025-11-23 from https://www.smhi.se/klimat/klimatet-da-ochnu/hur-var-vadret/G%C3%B6teborg/temperature

Tai, C.V., Kim, D., Kronenberg, R., Vorobevskii, I., & Luong, T.T. (2025). Beneath the surface: Exploring relationship between pluvial floods and income disparities for residential basements in Seoul, South Korea. *International Journal of Disaster Risk Reduction, 123*, 105501. https://doi.org/10.1016/j.ijdrr.2025.105501

Taramelli, A., Righini, M., Valentini, E., Alfieri, L., Gatti, I., & Gabellani, S. (2022). Buildingscale flood loss estimation through vulnerability pattern characterization: application to an urban flood in Milan, Italy. *Natural Hazards and Earth System Sciences, 22*, 3543–3569. https://doi.org/10.5194/nhess-22-3543-2022

Torgersen, G., Rød, J.K., Kvaal, K., Bjerkholt, J.T., & Lindholm O.G. (2017). Evaluating Flood Exposure for Properties in Urban Areas Using a Multivariate Modelling Technique. *Water, 9*(5), 318. https://doi.org/10.3390/w9050318

Trafikverket. (2025, May 3). *Dataproduktspecifikation – Bro och tunnel*. https://bransch.trafikverket.se/TrvSeFiler/Dataproduktspecifikationer/V%C3%A4gdata produk ter/DPS_A-B/1040Bro%20och%20tunnel.pdf

Trafikverket. (2025, March 5). *Dataproduktspecifikation – Tillgänglighetsvägnät*. https://bransch.trafikverket.se/TrvSeFiler/Dataproduktspecifikationer/V%C3%A4gdata produkter/DPS_S-T/1047Tillg%C3%A4nglighetsv%C3%A4gn%C3%A4t.pdf

Tsang, M., & Scott, D.M. (2020). An integrated approach to modeling the impact of floods on emergency services: A case study of Calgary, Alberta. *Journal of Transport Geography, 86,* 102774. https://doi.org/10.1016/j.jtrangeo.2020.102774

WSP. (2023). *KLIMATRELATERADE RISKER FÖR SKADOR PÅ DEN BYGGDA MILJÖN UNDERLAG TILL ÖVERSIKTSPLAN 2050 SÖDERTÄLJE KOMMUN.* Södertälje kommun.https://www.sodertalje.se/globalassets/sbk/oversiktsplan-2050/bilaga-2---klimatrelateraderisker-for-skador-pa-den-byggda-miljon.pdf

Yin, J., Yu, D., & Liao, B. (2020). A city-scale assessment of emergency response accessibility to vulnerable populations and facilities under normal and pluvial flood conditions for Shanghai, China. *Environment and Planning B: Urban Analytics and City Science 48*(8). https://doi.org/10.1177/2399808320971304

Zang, Y., Huang, J., & Wang, H. (2024). Dynamic impact assessment of urban floods on the compound spatial network of buildings-roads-emergency service facilities. *Science of The Total Environment, 926*, 172007. https://doi.org/10.1016/j.scitotenv.2024.172007

Zhou, R., Zheng, H., Liu, Y., Xie, G., & Wan, W. (2022). Flood impacts on urban road connectivity in southern China. *Scientific Reports, 12*, 16866. https://doi.org/10.1038/s41598022-20882-5

Series from Lund University

Department of Physical Geography and Ecosystem Science

Master Thesis in Geographical Information Science

1. *Anthony Lawther:* The application of GIS-based binary logistic regression for slope failure susceptibility mapping in the Western Grampian Mountains, Scotland (2008).
2. *Rickard Hansen:* Daily mobility in Grenoble Metropolitan Region, France. Applied GIS methods in time geographical research (2008).
3. *Emil Bayramov:* Environmental monitoring of bio-restoration activities using GIS and Remote Sensing (2009).
4. *Rafael Villarreal Pacheco:* Applications of Geographic Information Systems as an analytical and visualization tool for mass real estate valuation: a case study of Fontibon District, Bogota, Columbia (2009).
5. *Siri Oestreich Waage:* a case study of route solving for oversized transport: The use of GIS functionalities in transport of transformers, as part of maintaining a reliable power infrastructure (2010).
6. *Edgar Pimiento:* Shallow landslide susceptibility – Modelling and validation (2010).
7. *Martina Schäfer:* Near real-time mapping of floodwater mosquito breeding sites using aerial photographs (2010).
8. *August Pieter van Waarden-Nagel:* Land use evaluation to assess the outcome of the programme of rehabilitation measures for the river Rhine in the Netherlands (2010).
9. *Samira Muhammad:* Development and implementation of air quality data mart for Ontario, Canada: A case study of air quality in Ontario using OLAP tool. (2010).

10. *Fredros Oketch Okumu*: Using remotely sensed data to explore spatial and temporal relationships between photosynthetic productivity of vegetation and malaria transmission intensities in selected parts of Africa (2011).

11. *Svajunas Plunge:* Advanced decision support methods for solving diffuse water pollution problems (2011).

12. *Jonathan Higgins:* Monitoring urban growth in greater Lagos: A case study using GIS to monitor the urban growth of Lagos 1990 - 2008 and produce future growth prospects for the city (2011).

13. *Mårten Karlberg:* Mobile Map Client API: Design and Implementation for Android (2011).

14. *Jeanette McBride:* Mapping Chicago area urban tree canopy using color infrared imagery (2011).

15. *Andrew Farina:* Exploring the relationship between land surface temperature and vegetation abundance for urban heat island mitigation in Seville, Spain (2011).

16. *David Kanyari*: Nairobi City Journey Planner: An online and a Mobile Application (2011).

17. *Laura V. Drews:* Multi-criteria GIS analysis for siting of small wind power plants - A case study from Berlin (2012).

18. *Qaisar Nadeem:* Best living neighborhood in the city - A GIS based multi criteria evaluation of ArRiyadh City (2012).

19. *Ahmed Mohamed El Saeid Mustafa:* Development of a photo voltaic building rooftop integration analysis tool for GIS for Dokki District, Cairo, Egypt (2012).

20. *Daniel Patrick Taylor*: Eastern Oyster Aquaculture: Estuarine Remediation via Site Suitability and Spatially Explicit Carrying Capacity Modeling in Virginia's Chesapeake Bay (2013).

21. *Angeleta Oveta Wilson:* A Participatory GIS approach to *unearthing* Manchester's Cultural Heritage '*gold mine'* (2013).

22. *Ola Svensson:* Visibility and Tholos Tombs in the Messenian Landscape: A Comparative Case Study of the Pylian Hinterlands and the Soulima Valley (2013).

23. *Monika Ogden:* Land use impact on water quality in two river systems in South Africa (2013).

24. *Stefan Rova:* A GIS based approach assessing phosphorus load impact on Lake Flaten in Salem, Sweden (2013).

25. *Yann Buhot:* Analysis of the history of landscape changes over a period of 200 years. How can we predict past landscape pattern scenario and the impact on habitat diversity? (2013).

26. *Christina Fotiou:* Evaluating habitat suitability and spectral heterogeneity models to predict weed species presence (2014).

27. *Inese Linuza:* Accuracy Assessment in Glacier Change Analysis (2014).

28. *Agnieszka Griffin:* Domestic energy consumption and social living standards: a GIS analysis within the Greater London Authority area (2014).

29. *Brynja Guðmundsdóttir:* Detection of potential arable land with remote sensing and GIS - A Case Study for Kjósarhreppur (2014).

30. *Oleksandr Nekrasov:* Processing of MODIS Vegetation Indices for analysis of agricultural droughts in the southern Ukraine between the years 2000-2012 (2014).

31. *Sarah Tressel:* Recommendations for a polar Earth science portal in the context of Arctic Spatial Data Infrastructure (2014).

32. *Caroline Gevaert:* Combining Hyperspectral UAV and Multispectral Formosat-2 Imagery for Precision Agriculture Applications (2014).

33. *Salem Jamal-Uddeen:* Using GeoTools to implement the multi-criteria evaluation analysis - weighted linear combination model (2014).

34. *Samanah Seyedi-Shandiz:* Schematic representation of geographical railway network at the Swedish Transport Administration (2014).

35. *Kazi Masel Ullah:* Urban Land-use planning using Geographical Information System and analytical hierarchy process: case study Dhaka City (2014).

36. *Alexia Chang-Wailing Spitteler:* Development of a web application based on MCDA and GIS for the decision support of river and floodplain rehabilitation projects (2014).

37. *Alessandro De Martino:* Geographic accessibility analysis and evaluation of potential changes to the public transportation system in the City of Milan (2014).

38. *Alireza Mollasalehi:* GIS Based Modelling for Fuel Reduction Using Controlled Burn in Australia. Case Study: Logan City, QLD (2015).

39. *Negin A. Sanati:* Chronic Kidney Disease Mortality in Costa Rica; Geographical Distribution, Spatial Analysis and Non-traditional Risk Factors (2015).

40. *Karen McIntyre:* Benthic mapping of the Bluefields Bay fish sanctuary, Jamaica (2015).

41. *Kees van Duijvendijk:* Feasibility of a low-cost weather sensor network for agricultural purposes: A preliminary assessment (2015).

42. *Sebastian Andersson Hylander:* Evaluation of cultural ecosystem services using GIS (2015).

43. *Deborah Bowyer:* Measuring Urban Growth, Urban Form and Accessibility as Indicators of Urban Sprawl in Hamilton, New Zealand (2015).

44. *Stefan Arvidsson:* Relationship between tree species composition and phenology extracted from satellite data in Swedish forests (2015).

45. *Damián Giménez Cruz*: GIS-based optimal localisation of beekeeping in rural Kenya (2016).

46. *Alejandra Narváez Vallejo:* Can the introduction of the topographic indices in LPJ-GUESS improve the spatial representation of environmental variables? (2016).

47. *Anna Lundgren:* Development of a method for mapping the highest coastline in Sweden using breaklines extracted from high resolution digital elevation models (2016).

48. *Oluwatomi Esther Adejoro:* Does location also matter? A spatial analysis of social achievements of young South Australians (2016).

49. *Hristo Dobrev Tomov:* Automated temporal NDVI analysis over the Middle East for the period 1982 - 2010 (2016).

50. *Vincent Muller:* Impact of Security Context on Mobile Clinic Activities A GIS Multi Criteria Evaluation based on an MSF Humanitarian Mission in Cameroon (2016).

51. *Gezahagn Negash Seboka:* Spatial Assessment of NDVI as an Indicator of Desertification in Ethiopia using Remote Sensing and GIS (2016).

52. *Holly Buhler:* Evaluation of Interfacility Medical Transport Journey Times in Southeastern British Columbia. (2016).

53. *Lars Ole Grottenberg*: Assessing the ability to share spatial data between emergency management organisations in the High North (2016).

54. *Sean Grant:* The Right Tree in the Right Place: Using GIS to Maximize the Net Benefits from Urban Forests (2016).

55. *Irshad Jamal:* Multi-Criteria GIS Analysis for School Site Selection in Gorno-Badakhshan Autonomous Oblast, Tajikistan (2016).

56. *Fulgencio Sanmartín:* Wisdom-volkano: A novel tool based on open GIS and time-series visualization to analyse and share volcanic data (2016).

57. *Nezha Acil:* Remote sensing-based monitoring of snow cover dynamics and its influence on vegetation growth in the Middle Atlas Mountains (2016).

58. *Julia Hjalmarsson:* A Weighty Issue: Estimation of Fire Size with Geographically Weighted Logistic Regression (2016).

59. *Mathewos Tamiru Amato:* Using multi-criteria evaluation and GIS for chronic food and nutrition insecurity indicators analysis in Ethiopia (2016).

60. *Karim Alaa El Din Mohamed Soliman El Attar:* Bicycling Suitability in Downtown, Cairo, Egypt (2016).

61. *Gilbert Akol Echelai:* Asset Management: Integrating GIS as a Decision Support Tool in Meter Management in National Water and Sewerage Corporation (2016).

62. *Terje Slinning:* Analytic comparison of multibeam echo soundings (2016).

63. *Gréta Hlín Sveinsdóttir:* GIS-based MCDA for decision support: A framework for wind farm siting in Iceland (2017).

64. *Jonas Sjögren:* Consequences of a flood in Kristianstad, Sweden: A GIS-based analysis of impacts on important societal functions (2017).

65. *Nadine Raska:* 3D geologic subsurface modelling within the Mackenzie Plain, Northwest Territories, Canada (2017).

66. *Panagiotis Symeonidis*: Study of spatial and temporal variation of atmospheric optical parameters and their relation with PM 2.5 concentration over Europe using GIS technologies (2017).

67. *Michaela Bobeck:* A GIS-based Multi-Criteria Decision Analysis of Wind Farm Site Suitability in New South Wales, Australia, from a Sustainable Development Perspective (2017).

68. *Raghdaa Eissa*: Developing a GIS Model for the Assessment of Outdoor Recreational Facilities in New Cities Case Study: Tenth of Ramadan City, Egypt (2017).

69. *Zahra Khais Shahid*: Biofuel plantations and isoprene emissions in Svea and Götaland (2017).

70. *Mirza Amir Liaquat Baig*: Using geographical information systems in epidemiology: Mapping and analyzing occurrence of diarrhea in urban - residential area of Islamabad, Pakistan (2017).

71. *Joakim Jörwall*: Quantitative model of Present and Future well-being in the EU-28: A spatial Multi-Criteria Evaluation of socioeconomic and climatic comfort factors (2017).

72. *Elin Haettner*: Energy Poverty in the Dublin Region: Modelling Geographies of Risk (2017).

73. *Harry Eriksson*: Geochemistry of stream plants and its statistical relations to soil- and bedrock geology, slope directions and till geochemistry. A GIS-analysis of small catchments in northern Sweden (2017).

74. *Daniel Gardevärn:* PPGIS and Public meetings – An evaluation of public participation methods for urban planning (2017).

75. *Kim Friberg:* Sensitivity Analysis and Calibration of Multi Energy Balance Land Surface Model Parameters (2017).

76. *Viktor Svanerud:* Taking the bus to the park? A study of accessibility to green areas in Gothenburg through different modes of transport (2017).

77. *Lisa-Gaye Greene*: Deadly Designs: The Impact of Road Design on Road Crash Patterns along Jamaica's North Coast Highway (2017).

78. *Katarina Jemec Parker*: Spatial and temporal analysis of fecal indicator bacteria concentrations in beach water in San Diego, California (2017).

79. *Angela Kabiru*: An Exploratory Study of Middle Stone Age and Later Stone Age Site Locations in Kenya's Central Rift Valley Using Landscape Analysis: A GIS Approach (2017).

80. *Kristean Björkmann*: Subjective Well-Being and Environment: A GIS-Based Analysis (2018).

81. *Williams Erhunmonmen Ojo*: Measuring spatial accessibility to healthcare for people living with HIV-AIDS in southern Nigeria (2018).

82. *Daniel Assefa*: Developing Data Extraction and Dynamic Data Visualization (Styling) Modules for Web GIS Risk Assessment System (WGRAS). (2018).

83. *Adela Nistora*: Inundation scenarios in a changing climate: assessing potential impacts of sea-level rise on the coast of South-East England (2018).

84. *Marc Seliger*: Thirsty landscapes - Investigating growing irrigation water consumption and potential conservation measures within Utah's largest master-planned community: Daybreak (2018).

85. *Luka Jovičić*: Spatial Data Harmonisation in Regional Context in Accordance with INSPIRE Implementing Rules (2018).

86. *Christina Kourdounouli*: Analysis of Urban Ecosystem Condition Indicators for the Large Urban Zones and City Cores in EU (2018).

87. *Jeremy Azzopardi*: Effect of distance measures and feature representations on distance-based accessibility measures (2018).

88. *Patrick Kabatha*: An open source web GIS tool for analysis and visualization of elephant GPS telemetry data, alongside environmental and anthropogenic variables (2018).

89. *Richard Alphonce Giliba*: Effects of Climate Change on Potential Geographical Distribution of Prunus africana (African cherry) in the Eastern Arc Mountain Forests of Tanzania (2018).

90. *Eiður Kristinn Eiðsson*: Transformation and linking of authoritative multi-scale geodata for the Semantic Web: A case study of Swedish national building data sets (2018).

91. *Niamh Harty*: HOP!: a PGIS and citizen science approach to monitoring the condition of upland paths (2018).

92. *José Estuardo Jara Alvear*: Solar photovoltaic potential to complement hydropower in Ecuador: A GIS-based framework of analysis (2018).

93. *Brendan O'Neill*: Multicriteria Site Suitability for Algal Biofuel Production Facilities (2018).

94. *Roman Spataru*: Spatial-temporal GIS analysis in public health – a case study of polio disease (2018).

95. *Alicja Miodońska*: Assessing evolution of ice caps in Suðurland, Iceland, in years 1986 - 2014, using multispectral satellite imagery (2019).

96. *Dennis Lindell Schettini*: A Spatial Analysis of Homicide Crime's Distribution and Association with Deprivation in Stockholm Between 2010-2017 (2019).

97. *Damiano Vesentini*: The Po Delta Biosphere Reserve: Management challenges and priorities deriving from anthropogenic pressure and sea level rise (2019).

98. *Emilie Arnesten*: Impacts of future sea level rise and high water on roads, railways and environmental objects: a GIS analysis of the potential effects of increasing sea levels and highest projected high water in Scania, Sweden (2019).

99. *Syed Muhammad Amir Raza*: Comparison of geospatial support in RDF stores: Evaluation for ICOS Carbon Portal metadata (2019).

100. *Hemin Tofiq*: Investigating the accuracy of Digital Elevation Models from UAV images in areas with low contrast: A sandy beach as a case study (2019).

101. *Evangelos Vafeiadis*: Exploring the distribution of accessibility by public transport using spatial analysis. A case study for retail concentrations and public hospitals in Athens (2019).

102. *Milan Sekulic*: Multi-Criteria GIS modelling for optimal alignment of roadway by-passes in the Tlokweng Planning Area, Botswana (2019).

103. *Ingrid Piirisaar*: A multi-criteria GIS analysis for siting of utility-scale photovoltaic solar plants in county Kilkenny, Ireland (2019).

104. *Nigel Fox*: Plant phenology and climate change: possible effect on the onset of various wild plant species' first flowering day in the UK (2019).

105. *Gunnar Hesch*: Linking conflict events and cropland development in Afghanistan, 2001 to 2011, using MODIS land cover data and Uppsala Conflict Data Programme (2019).

106. *Elijah Njoku*: Analysis of spatial-temporal pattern of Land Surface Temperature (LST) due to NDVI and elevation in Ilorin, Nigeria (2019).

107. *Katalin Bunyevácz*: Development of a GIS methodology to evaluate informal urban green areas for inclusion in a community governance program (2019).

108. *Paul dos Santos*: Automating synthetic trip data generation for an agent-based simulation of urban mobility (2019).

109. *Robert O' Dwyer*: Land cover changes in Southern Sweden from the mid-Holocene to present day: Insights for ecosystem service assessments (2019).

110. *Daniel Klingmyr*: Global scale patterns and trends in tropospheric NO2 concentrations (2019).

111. *Marwa Farouk Elkabbany*: Sea Level Rise Vulnerability Assessment for Abu Dhabi, United Arab Emirates (2019).

112. *Jip Jan van Zoonen*: Aspects of Error Quantification and Evaluation in Digital Elevation Models for Glacier Surfaces (2020).

113. *Georgios Efthymiou*: The use of bicycles in a mid-sized city – benefits and obstacles identified using a questionnaire and GIS (2020).

114. *Haruna Olayiwola Jimoh*: Assessment of Urban Sprawl in MOWE/IBAFO Axis of Ogun State using GIS Capabilities (2020).

115. *Nikolaos Barmpas Zachariadis*: Development of an iOS, Augmented Reality for disaster management (2020).

116. *Ida Storm*: ICOS Atmospheric Stations: Spatial Characterization of CO2 Footprint Areas and Evaluating the Uncertainties of Modelled CO2 Concentrations (2020).

117. *Alon Zuta*: Evaluation of water stress mapping methods in vineyards using airborne thermal imaging (2020).

118. *Marcus Eriksson*: Evaluating structural landscape development in the municipality Upplands-Bro, using landscape metrics indices (2020).

119. *Ane Rahbek Vierø*: Connectivity for Cyclists? A Network Analysis of Copenhagen's Bike Lanes (2020).

120. *Cecilia Baggini*: Changes in habitat suitability for three declining Anatidae species in saltmarshes on the Mersey estuary, North-West England (2020).

121. *Bakrad Balabanian*: Transportation and Its Effect on Student Performance (2020).

122. *Ali Al Farid*: Knowledge and Data Driven Approaches for Hydrocarbon Microseepage Characterizations: An Application of Satellite Remote Sensing (2020).

123. *Bartlomiej Kolodziejczyk*: Distribution Modelling of Gene Drive-Modified Mosquitoes and Their Effects on Wild Populations (2020).

124. *Alexis Cazorla*: Decreasing organic nitrogen concentrations in European water bodies - links to organic carbon trends and land cover (2020).

125. *Kharid Mwakoba*: Remote sensing analysis of land cover/use conditions of community-based wildlife conservation areas in Tanzania (2021).

126. *Chinatsu Endo*: Remote Sensing Based Pre-Season Yellow Rust Early Warning in Oromia, Ethiopia (2021).

127. *Berit Mohr*: Using remote sensing and land abandonment as a proxy for long-term human out-migration. A Case Study: Al-Hassakeh Governorate, Syria (2021).

128. *Kanchana Nirmali Bandaranayake*: Considering future precipitation in delineation locations for water storage systems - Case study Sri Lanka (2021).

129. *Emma Bylund*: Dynamics of net primary production and food availability in the aftermath of the 2004 and 2007 desert locust outbreaks in Niger and Yemen (2021).

130. *Shawn Pace*: Urban infrastructure inundation risk from permanent sea-level rise scenarios in London (UK), Bangkok (Thailand) and Mumbai (India): A comparative analysis (2021).

131. *Oskar Evert Johansson*: The hydrodynamic impacts of Estuarine Oyster reefs, and the application of drone technology to this study (2021).

132. *Pritam Kumarsingh*: A Case Study to develop and test GIS/SDSS methods to assess the production capacity of a Cocoa Site in Trinidad and Tobago (2021).

133. *Muhammad Imran Khan*: Property Tax Mapping and Assessment using GIS (2021).

134. *Domna Kanari*: Mining geosocial data from Flickr to explore tourism patterns: The case study of Athens (2021).

135. *Mona Tykesson Klubien*: Livestock-MRSA in Danish pig farms (2021).

136. *Ove Njøten*: Comparing radar satellites. Use of Sentinel-1 leads to an increase in oil spill alerts in Norwegian waters (2021).

137. *Panagiotis Patrinos*: Change of heating fuel consumption patterns produced by the economic crisis in Greece (2021).

138. *Lukasz Langowski*: Assessing the suitability of using Sentinel-1A SAR multi-temporal imagery to detect fallow periods between rice crops (2021).

139. *Jonas Tillman*: Perception accuracy and user acceptance of legend designs for opacity data mapping in GIS (2022).

140. *Gabriela Olekszyk*: ALS (Airborne LIDAR) accuracy: Can potential low data quality of ground points be modelled/detected? Case study of 2016 LIDAR capture over Auckland, New Zealand (2022).

141. *Luke Aspland*: Weights of Evidence Predictive Modelling in Archaeology (2022).

142. *Luís Fareleira Gomes*: The influence of climate, population density, tree species and land cover on fire pattern in mainland Portugal (2022).

143. *Andreas Eriksson*: Mapping Fire Salamander (Salamandra salamandra) Habitat Suitability in Baden-Württemberg with Multi-Temporal Sentinel-1 and Sentinel-2 Imagery (2022).

144. *Lisbet Hougaard Baklid*: Geographical expansion rate of a brown bear population in Fennoscandia and the factors explaining the directional variations (2022).

145. *Victoria Persson*: Mussels in deep water with climate change: Spatial distribution of mussel (Mytilus galloprovincialis) growth offshore in the French Mediterranean with respect to climate change scenario RCP 8.5 Long Term and Integrated Multi-Trophic Aquaculture (IMTA) using Dynamic Energy Budget (DEB) modelling (2022).

146. *Benjamin Bernard Fabien Gérard Borgeais*: Implementing a multi-criteria GIS analysis and predictive modelling to locate Upper Palaeolithic decorated caves in the Périgord noir, France (2022).

147. *Bernat Dorado-Guerrero*: Assessing the impact of post-fire restoration interventions using spectral vegetation indices: A case study in El Bruc, Spain (2022).

148. *Ignatius Gabriel Aloysius Maria Perera*: The Influence of Natural Radon Occurrence on the Severity of the COVID-19 Pandemic in Germany: A Spatial Analysis (2022).

149. *Mark Overton*: An Analysis of Spatially-enabled Mobile Decision Support Systems in a Collaborative Decision-Making Environment (2022).

150. *Viggo Lunde*: Analysing methods for visualizing time-series datasets in open-source web mapping (2022).

151. *Johan Viscarra Hansson*: Distribution Analysis of Impatiens glandulifera in Kronoberg County and a Pest Risk Map for Alvesta Municipality (2022).

152. *Vincenzo Poppiti*: GIS and Tourism: Developing strategies for new touristic flows after the Covid-19 pandemic (2022).

153. *Henrik Hagelin*: Wildfire growth modelling in Sweden - A suitability assessment of available data (2023).

154. *Gabriel Romeo Ferriols Pavico*: Where there is road, there is fire (influence): An exploratory study on the influence of roads in the spatial patterns of Swedish wildfires of 2018 (2023).

155. *Colin Robert Potter*: Using a GIS to enable an economic, land use and energy output comparison between small wind powered turbines and large-scale wind farms: the case of Oslo, Norway (2023).

156. *Krystyna Muszel*: Impact of Sea Surface Temperature and Salinity on Phytoplankton blooms phenology in the North Sea (2023).

157. *Tobias Rydlinge*: Urban tree canopy mapping - an open source deep learning approach (2023).

158. *Albert Wellendorf*: Multi-scale Bark Beetle Predictions Using Machine Learning (2023).

159. *Manolis Papadakis*: Use of Satellite Remote Sensing for Detecting Archaeological Features: An Example from Ancient Corinth, Greece (2023).

160. *Konstantinos Sourlamtas*: Developing a Geographical Information System for a water and sewer network, for monitoring, identification and leak repair - Case study: Municipal Water Company of Naoussa, Greece (2023).

161. *Xiaoming Wang*: Identification of restoration hotspots in landscape-scale green infrastructure planning based on model-predicted connectivity forest (2023).

162. *Sarah Sienaert*: Usability of Sentinel-1 C-band VV and VH SAR data for the detection of flooded oil palm (2023).

163. *Katarina Ekeroot*: Uncovering the spatial relationships between Covid-19 vaccine coverage and local politics in Sweden (2023).

164. *Nikolaos Kouskoulis*: Exploring patterns in risk factors for bark beetle attack during outbreaks triggered by drought stress with harvester data on attacked trees: A case study in Southeastern Sweden (2023).

165. *Jonas Almén*: Geographic polarization and clustering of partisan voting: A local-level analysis of Stockholm Municipality (2023).

166. *Sara Sharon Jones*: Tree species impact on Forest Fire Spread Susceptibility in Sweden (2023).

167. *Takura Matswetu*: Towards a Geographic Information Systems and Data-Driven Integration Management. Studying holistic integration through spatial accessibility of services in Tampere, Finland. (2023).

168. *Duncan Jones*: Investigating the influence of the tidal regime on harbour porpoise *Phocoena phocoena* distribution in Mount's Bay, Cornwall (2023).

169. *Jason Craig Joubert*: A comparison of remote sensed semi-arid grassland vegetation anomalies detected using MODIS and Sentinel-3, with anomalies in ground-based eddy covariance flux measurements (2023).

170. *Anastasia Sarelli*: Land cover classification using machine-learning techniques applied to fused multi-modal satellite imagery and time series data (2024).

171. *Athanasios Senteles*: Integrating Local Knowledge into the Spatial Analysis of Wind Power: The case study of Northern Tzoumerka, Greece (2024).

172. *Rebecca Borg:* Using GIS and satellite data to assess access of green area for children living in growing cities (2024).

173. *Panagiotis–Dimitrios Tsachageas*: Multicriteria Evaluation in Real Estate Land-use Suitability Analysis: The case of Volos, Greece (2024).

174. *Hugo Nilsson*: Inferring lane-level topology of signalised intersections from aerial imagery and OpenStreetMap using deep learning (2024).

175. *Pavlos Alexantonakis*: Estimating lake water volume fluctuations using Sentinel-2 and ICESat-2 remote sensing data (2024).

176. *Karl-Martin Wigen*: Physical barriers and where to find them (2024).

177. *Martin Storsnes*: Temporal RX-algorithm performance on Sentinel-2 images (2024).

178. *Saulė Gabrielė Petraitytė*: The Relation Between Covid-19 Vaccination and Voting Trends in Lithuania: A Spatial Analysis (2024).

179. *Pedro Martinez Duran*: Olive yield forecasting from remote sensing and climate datasets in the Jaen province (Spain) (2024).

180. *Josefine Kynde Hämberg*: Proximity to Urban Green Spaces for Older Adults in Specific Housings - a Case Study of Malmö, Sweden (2024).

181. *Max Bengtsson*: A Site Selection of An Energy Island in the North Sea: Optimal Location in an Ecological and an Economic Scenario Using a Multicriteria Decision Analysis (MCDA) (2024).

182. *Anna Börmann*: Assessing Great Britain as a relocation site for the threatened Iberian Lynx in a changing climate (2024).

183. *Josephine Roosli*: Flood Risk Assessment for the Kävlinge River for Present and Future Climate Scenarios using HEC-RAS Rain-on-Grid (2024).

184. *Seán Flanagan*: Spatiotemporal dynamics of E-scooter sharing ridership and their associations with the built environment: A Swedish comparative study (2024).

185. *Wouter Vorsters*: Assessing the Impact of Combined Sewer Overflow on the Habitat of Lampetra planeri: A Case Study in Flanders, Belgium (2025).

186. *Kathleen Macdonald*: Cetacean strandings on the Scottish coast: coastal accessibility factors lead to underreporting (2025).

187. *Athanasios Emmanouil Mourampetzis*: Navigating the Shadows: A Comparative Analysis of SAR and Optical Imagery for Detecting (Dark) Vessels (2025).

188. *Nizam-ud-Din*: Spatial Land Records System using Geospatial Techniques: a case study of a Mid-Sized Village in Pakistan (2025).

189. *Nedim Nasic Kjellgren*: Linked Geodata: Improving Rooftop Photovoltaic Production Estimates through BIM-GIS Integration using Semantic Web Technologies (2025).

190. *Vedrana Pretkovic*: Spatio-temporal vegetation changes in the Pacific-Chocó region of Colombia during the conflict and post-conflict periods (2025).

191. *Evelina Bengtsson*: A Socioeconomic Dimension of Crime: A Spatial Study of Firearm-related Violence in Malmö (2025).

192. *Martynas Bielinis*: Application of C-band Radar Interferometry for Dune Monitoring in the Curonian Spit (2025).

193. *Paulina Magdalena Rieke*: Case study of the benefits of BIM and GIS solutions used on a live infrastructure project (2025).

194. *Alina Schärer*: Evaluating the Impact of Urban Green Spaces and Vegetation Characteristics on Land Surface Temperature Across Swiss Cities Using Machine Learning (2025).

195. *Paul Stewart:* Where is wild in Glasgow's Southside? A test of the applicability of relative wildness mapping to suburban Scotland (2025).

196. *Georgios Fylakis:* Spatiotemporal analysis of the integration between shared e-scooters and public transport: Case studies in Oslo and Stockholm (2025).

197. *Andreas Klasson*: Generating 3D building models according to Swedish building specification using footprints and airborne laser scanning (2025).

198. *Agaton Järemo Lawin*: The spread of Japanese knotweed in Scania: Invasion suitability prediction using species distribution modelling (2025).

199. *Jesse Stewart:* Contextualizing the Geographic Influence on Infantry Manoeuvrability in a Historical Battlefield Using GIS: A Case Study of the Canadian Corps in the Second Battle of Passchendaele, First World War (2025).

200. *Oskar Vejkdal Thorsberg*: Automatic geometry extraction in digital building permits: A case study using BIM and NS Building (2025).

201. *Spyridon Gerafentis*: Impact of the COVID-19 "Lockdown" on Air Quality in Athens (2025).

202. *Symeon Andriotis*: Political Violence in Athens, Greece (2008-2024): A Machine Learning Approach for Predictive Modelling of Spatial Risk Patterns (2025).

203. *Simon Westman*: Detecting Structurally Old Scots Pine: A Crown-Metric Approach Using National ALS and LIFT Enrichment (2026).

204. *Freja Randeris Kristoffersen*: Satellite-Derived Bathymetry of Danish Coastal Waters Using Machine Learning with Sentinel-2 and ICESat-2 data (2026).

205. *Markus Honkanen*: Securitas Per Scientiam: GIS-MCDA of Civil Defence Shelter Distribution Efficiency in the Helsinki Capital Region (2026).

206. *Amanda Carolina Santos Motta*: Visualization Tools for Simulation Results Based on 3D City Models: An Urban Planner-Focused Study (2026).

207. *Gintars Krumins*: Mapping forest felling activities in Latvia from Sentinel-2 satellite imagery using machine learning (2026).

208. *Jenny Berntsson*: Using Multi-criteria GIS analysis in nature conservation planning in Lilla Edet municipality (2026).

209. *Sebastian Daland*: Flood impacts on road accessibility and buildings in Gothenburg during a 100-year rainfall event (2026).